FAA-RD-75-234

Project Report
ATC-61

Empirical Characterization of IPC Tracker Performance Using DABS Data

J. L. Leeper
A. A. Tvirbutas

9 June 1976

Lincoln Laboratory
MASSACHUSETTS INSTITUTE OF TECHNOLOGY
LEXINGTON, MASSACHUSETTS

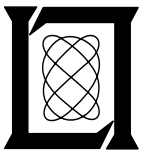

Prepared for the Federal Aviation Administration,
Washington, D.C. 20591

This document is available to the public through
the National Technical Information Service,
Springfield, VA 22161

Report No. FAA-RD-75-234

ERRATA SHEET

for

PROJECT REPORT ATC-61

EMPIRICAL CHARACTERIZATION OF IPC TRACKER
PERFORMANCE USING DABS DATA
9 June 1976

On cover and form DOT F 1700.7 please change the FAA-RD number from FAA-RD-76-2 to FAA-RD-75-234.

15 July 1976

Publications Office
M.I.T. Lincoln Laboratory
P.O. Box 73
Lexington, Massachusetts 02173

Technical Report Documentation Page

1. Report No.	2. Government Accession No.	3. Recipient's Catalog No.
FAA-RD-76-2		

4. Title and Subtitle	5. Report Date
Empirical Characterization of IPC Tracker Performance Using DABS Data	9 June 1976
	6. Performing Organization Code

7. Author(s)	8. Performing Organization Report No.
J. L. Leeper (Lincoln Laboratory) A. A. Tvirbutas (Arcon Corporation)	ATC-61

9. Performing Organization Name and Address	10. Work Unit No. (TRAIS) 45364 Project No. 034-241-012
Massachusetts Institute of Technology Lincoln Laboratory P.O. Box 73 Lexington, Massachusetts 02173	11. Contract or Grant No. DOT-FA72-WAI-261
	13. Type of Report and Period Covered Interim Project Report
12. Sponsoring Agency Name and Address Department of Transportation Federal Aviation Administration Systems Research and Development Service Washington, D.C. 20591	14. Sponsoring Agency Code

15. Supplementary Notes

The work reported in this document was performed at Lincoln Laboratory, a center for research operated by Massachusetts Institute of Technology, under Air Force Contract F19628-76-C-0002.

16. Abstract

The performance of a set of tracker algorithms proposed for use in the DABS-based Intermittent Positive Control (IPC) collision avoidance system is assessed. The position projecting tracker algorithms are subjected to actual surveillance data obtained at the Lincoln Laboratory DABS Experimental Facility. Effects of turn-rate, speed, wind and surveillance accuracy upon heading error, speed error and position error are presented.

17. Key Words	18. Distribution Statement
Air Traffic Control Intermittent positive control Tracker performance Simulation Heading error Position error Algorithm	Document is available to the public through the National Technical Information Service, Springfield, Virginia 22151.

19. Security Classif. (of this report)	20. Security Classif. (of this page)	21. No. of Pages	
Unclassified	Unclassified	84	

Form DOT F 1700.7 (8-72) Reproduction of completed page authorized

Table of contents

List of illustrations

List of illustrations (cont.)

List of Illustrations (cont.)

List of Tables

EMPIRICAL CHARACTERIZATION OF IPC TRACKER PERFORMANCE USING DABS DATA

1.0 INTRODUCTION

Intermittent Positive Control (IPC), a ground based aircraft warning and collision avoidance system, utilizing surveillance data from beacon equipped aircraft, is presently being evaluated at Lincoln Laboratory. The evaluation system uses the Lincoln Laboratory experimental sensor (DABSEF) augmented with IPC software and various display and communication items necessary to direct and monitor the test aircraft. The conflict warning and resolution system concept requires that the IPC equipped sensor be capable of identifying and communicating (via data link) with each test aircraft, and the sensor be capable of accurately projecting the future position, velocity, and altitude of each aircraft, whether or not it is following a straight line, turning, climbing or descending flight path.

The portion of the IPC software involved with the dynamic projection of aircraft position, speed, and altitude is referred to as "the IPC tracker." This report, covering the initial phase of the IPC tracker study, characterizes the performance of an early version of the IPC tracker software, the basic logic for which is described in Reference 1.

The approach taken in this part of the study was to:

(a) Define two standard or reference trajectories representing typical ideal and non-ideal turns; identifying each surveillance point (scan) along the turn (see Appendix A)

(b) Perturb each datum of the set representing the turns with the range and angular uncertainties of the test sensor (DABSEF) by adding system noise

(c) Repeatedly subject the tracker model (set of specified algorithms with specified threshold, etc., parameters) to the perturbed turn trajectories (simulated surveillance data at each designated scan)

(c) Plot the expected tracker performance during these turns in terms of both rms and dynamic (scan by scan) position, velocity, and altitude errors.

Section 2.0 of this report details the methods used to depict tracker performance, describes the effects of thresholding, and presents the results of performance simulation runs based upon ideal turn inputs perturbed by surveillance uncertainties and Gaussian noise. Section 3.0 presents a description of the result of simulation runs using a non-ideal turn (including

effect of wind, speed changes, etc.), and Section 4. 0 recommends several improvements in the tracker, based on the performance of the present tracker.

2.0 TRACKER PERFORMANCE FOR IDEALIZED TURNS

2.1 Methods of Depicting Tracker Performance

The principal measures used to assess the IPC tracker performance during the IPC evaluation study were heading error, speed error, and position error. Each simulation run repeatedly subjected the tracker to surveillance data as would have been provided by a "typical" DABS sensor attempting to track the aircraft. The surveillance azimuth and range data to be tracked differ from that of the true turn by the surveillance inaccuracy (or uncertainty) introduced by the sensor in a random manner. In order to summarize the results of numerous flights along the randomly perturbed turn to which the tracker was subjected during one simulation run, errors existing at the time, corresponding to a particular sensor "scan," may be root-mean-squared. Or, as has been done in this study, the "dynamic error performance" of the tracker may be depicted by plotting the actual distribution of the tracking errors for each scan during the turn. Figures 2-1(a) and 2-1(b) illustrate the "rms" and "dynamic" presentations of tracker heading performance for the same simulation.

The root-mean-squared errors provide an approximation to the tracker average performance, but such averaging can be misleading in many situations as may be seen by comparing Figs. 2-1(a) and 2-1(b). Note that between scans 18 and 50, the tracker exhibits two different types of response, e.g., in scan 21 approximately one-half the cases exhibit a heading error of -22°, and the remaining cases exhibit an error of -7°. This dual-mode response of the tracker is caused by the nonlinearity of the tracker in declaring turns. Figure 2-2 indicates that the tracker was not predominantly in a turn detection mode in any single scan.

2.2 Effects of Thresholding

Figure 2-3(a), which indicates the scan-by-scan cross-track measurement error and the corresponding threshold value, illustrates the effect of the threshold mechanism on tracker response. No measurement noise is used in this example in order to demonstrate the tracker response under ideal conditions. It is noted that the threshold values change from scan to scan as a result of changes in the tracker heading and speed estimates. The pronounced drop in the residual value at scan 24 corresponds to the heading correction produced by the turn declaration. This drop indicates (for this particular case) that the heading lag prior to turn detection which caused the residual to be high also delayed the ideal turn detection by several scans.

By superimposing a data uncertainty on several individual points of the trajectory, it is possible to show how noise affects turn declaration. For example, assume that noise is superimposed on the trajectory during scans 18, and 20, respectively. A simplifying assumption is made that data uncertainty does not affect the trajectory previous to scans 18 and 20, respectively.

With Gaussian noise superimposed during scan 18, a turn would be declared approximately 15% of the time. With Gaussian noise superimposed during scan 20, a turn would be declared approximately 31% of the time.

The behavior depicted in Fig. 2-3 provides some insight into the set of characteristics presented in Figs. 2-1(a) and 2-1(b). Figure 2-1(b) illustrates the effect of uncertainties on turn declaration in an actual case. Turn declaration starts during scan 18; and by scan 21, turns have been declared for all 30 cases. As a turn is declared, the cross-track deviation is reduced sufficiently to disable the threshold, and several scans are necessary for the error to build again. This intermittent nature of turn declaration produces a nonregular behavior in the rms heading error (Fig. 2-1(a)). The rms heading error is therefore directly related to the percentage of turn declarations generated during a scan. This situation is especially obvious between scans 18 and 35 in Fig. 2-1(a).

Figure 2-3(b) is an example of the threshold behavior for a more realistic turn rate. (An ideal, no noise case is again chosen.) The turn is declared in this case during scan 15 (rather than scan 23 for a turn rate of 1.5°/sec in Fig. 2-3(a)). Although the turn declaration produces a change in tracker heading, position and speed estimates are not directly modified by turn declaration. Position errors are reduced in subsequent scans through the normal linear filter gains as a result of improved heading. The linear filter correction is not sufficient in this case to suppress turn detection on the subsequent scan 16.

For low-speed aircraft and low turn rates as exemplified in Figs. 2-3(a), and 2-3(b), the turn declarations are delayed for several scans and are also intermittent. This behavior is caused by the high values assumed for the tracker azimuth and range uncertainties (range (R) sigma of 150 ft; azimuth sigma of 0.1°). In view of the fact that the simulation utilizes the actual DABSEF measurement uncertainties of 0.04° and 30 ft, it is expected that the tracker will exhibit a less than optimal response in turns.

Table 2-1 indicates the type of delay observed in detecting turns for which perfect data is provided. For the cases indicated, the turn detection mechanism does not declare a turn until the aircraft is at least one scan into the turn maneuver. As the speed and turn rates decrease, the delay increases.

TABLE 2-1. TURN DECLARATION DELAY (scans)
(No measurement errors)

Speed (knots)	Turn Rate (deg/sec) 1	1.5	3	4	5	6	7
100	-	12	4	3	3	2	2
200	14	5	3	2	2	2	1
300	7	4	2	2	1	1	1
400	5	4	2	2	1	1	1

Range = 20 nmi
Start of turn (scan 10)
End of turn (scan 25)

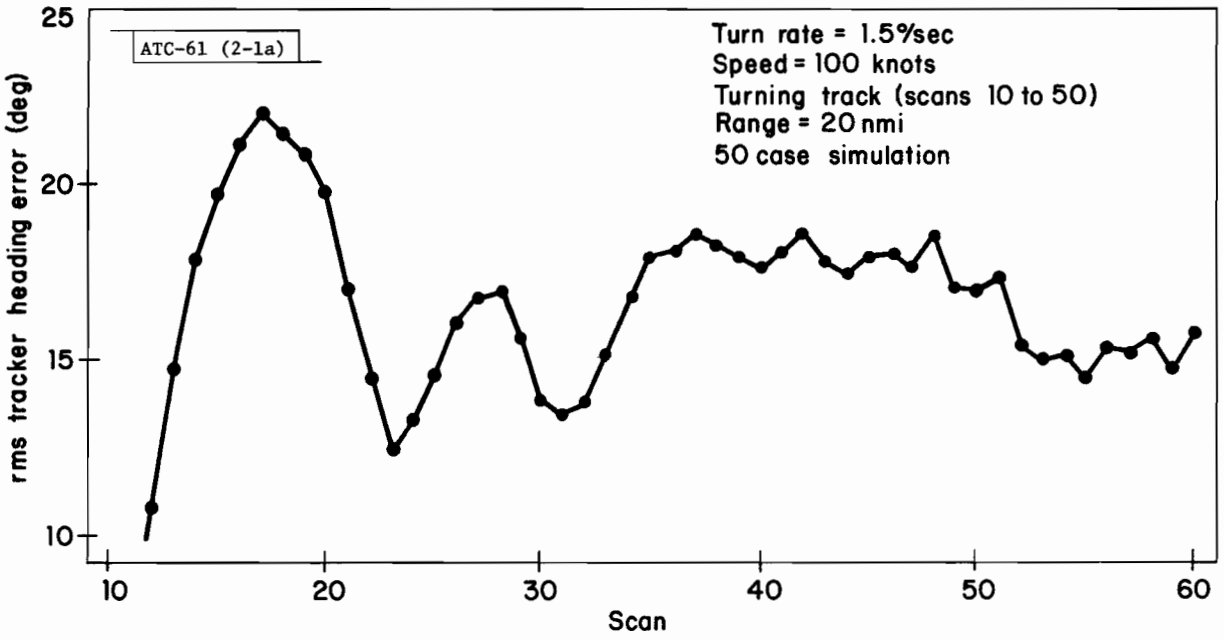

Fig. 2-1(a). Heading error vs scan (1.5°/sec turn rate).

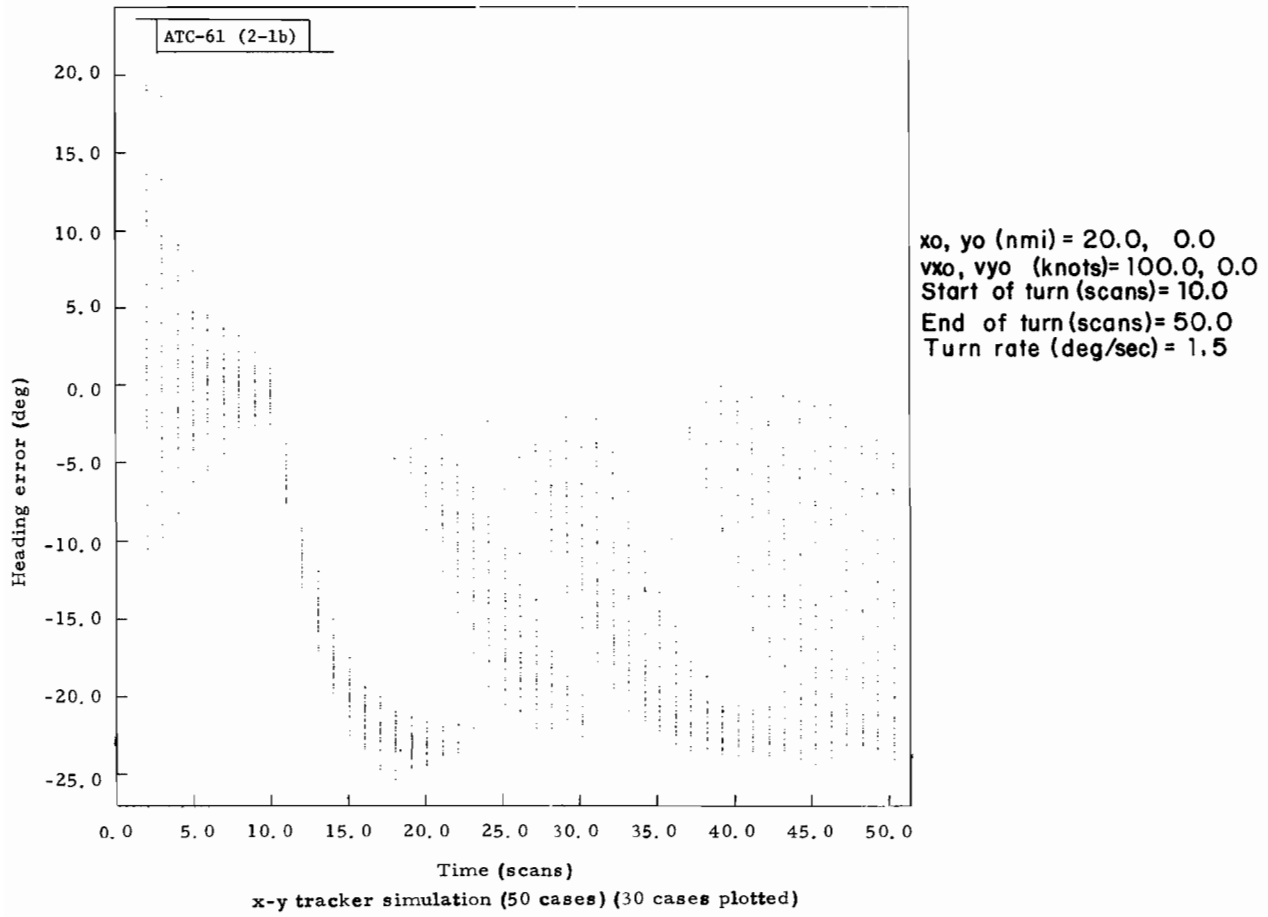

Fig. 2-1(b). Dynamic heading error vs scan (1.5°/sec turn rate).

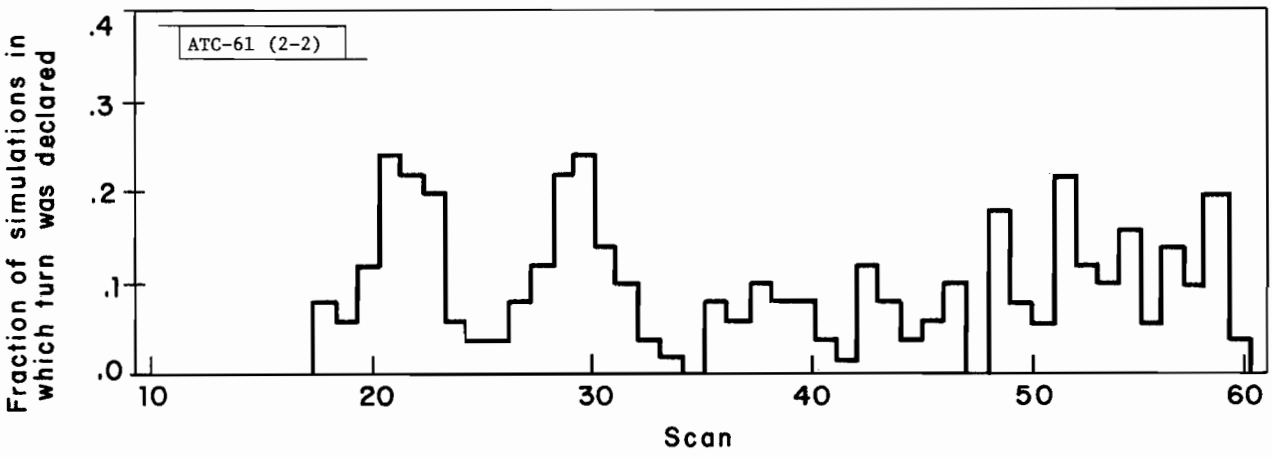

Fig. 2-2. Percentage of simulation in which a turn was declared vs scan.

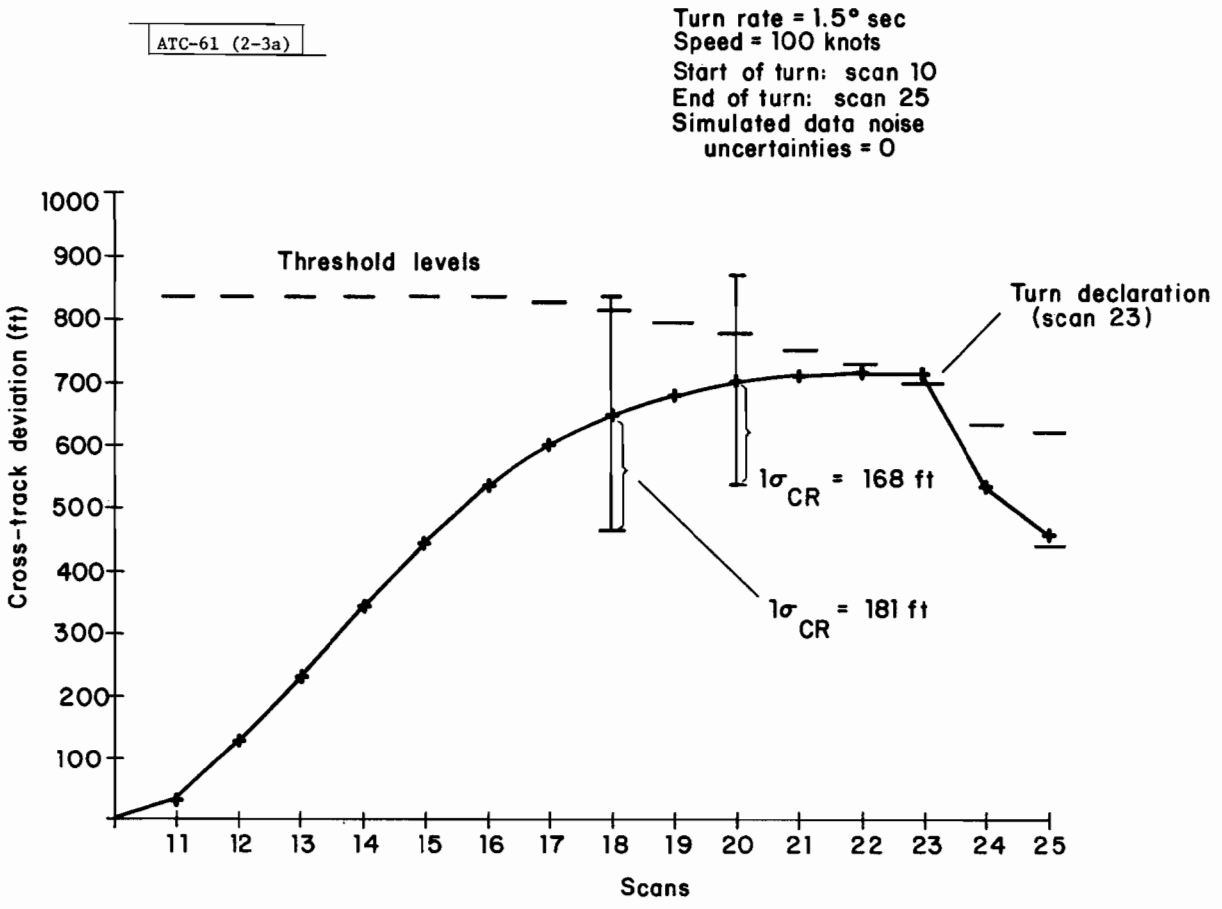

Fig. 2-3(a). Turn declaration; low turn rate (1.5°/sec turn rate; ideal noise).

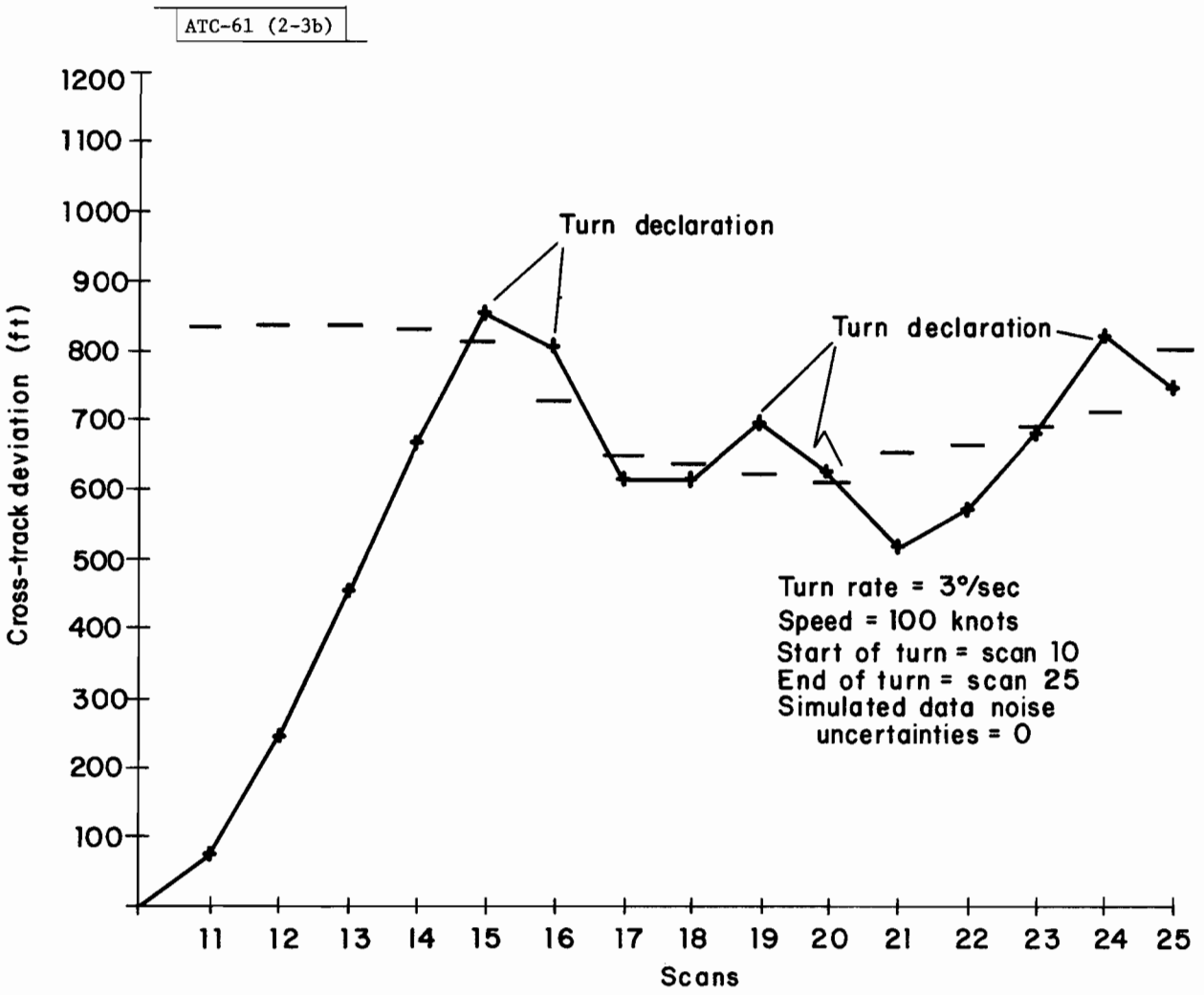

Fig. 2-3(b). Turn declaration; typical turn rate (3.0°/sec turn rate; ideal noise).

2.3 Tracker Behavior Modes

The turn detection mechanism results in a tracker response that is correlated to the mode in which the turn detection is operating. If no turns are declared, the tracker utilizes the basic α-β filtering. For low turn rates, it is not uncommon for the tracker to operate in this mode and follow the turn without making a turn declaration. For high turn rates, the tracker declares a turn after a delay of 1 or 2 scans and continues to declare the turn throughout the remainder of the turn maneuver. After the turn is declared, the tracker uses the heading correction procedure in addition to the basic α-β tracking. The cases of no-turn detection and "saturated" turn detection represent two extremes in tracker behavior. Between these extremes, the turn declarations are intermittent and are not unique. In this region, different values of measurement noise, superimposed on the same trajectory, produce different triggering sequences.

Figure 2-4 illustrates the different modes of tracker operation for a variety of turn rates and velocities. Each data point represents a simulation of 250 cases for an aircraft 20 nmi from the sensor following the simulation reference turn described in Appendix A (Fig. A-1). Each simulation operates from scan 1 to scan 50; the turn starting at scan 10 and ending at scan 25. The vertical axis in Fig. 2-4 represents the average number of turn declarations issued by the tracker during the turn maneuvers. The data for the 400-knot airspeed best demonstrate the transition of the tracker behavior between the linear operation area and the saturated turn detection area. At the 0.8^{o}/sec turn rate, some turn declarations begin to occur. The average number of turn declarations, however, is still less than 1; consequently, only certain data conditions determine when the tracker begins to declare turns. As the turn rate increases, the number of turn declarations increases until a turn rate of 2.5^{o} is reached. The tracker is basically "locked in" on the turn at this point, and as the turn rate increases, the average number of turn declarations converge to 14. Figure 2-4 has been divided into five modes (regions) of behavior. As mentioned previously, the region between saturation and no-turn declaration encompasses possible intermittent turn declaration sequences. It is useful to make some distinction between the types of behavior in the region between saturation and no-turn declaration, in view of the fact that it contains a large percentage of the realistic aircraft maneuvers. This region is subdivided into Regions 2, 3, and 4 in Fig. 2-4. The following is a description of the subdivisions.

Region 1: Saturation Mode. Whenever a turn is declared, the declaration mechanism is "on" during the duration of the turn.

Region 2: Weak Saturation Mode. Whenever a turn is declared, the turn declaration mechanism is "on" during a substantial part of the turn. (For shorter turns, this region would correspond to Region 1.)

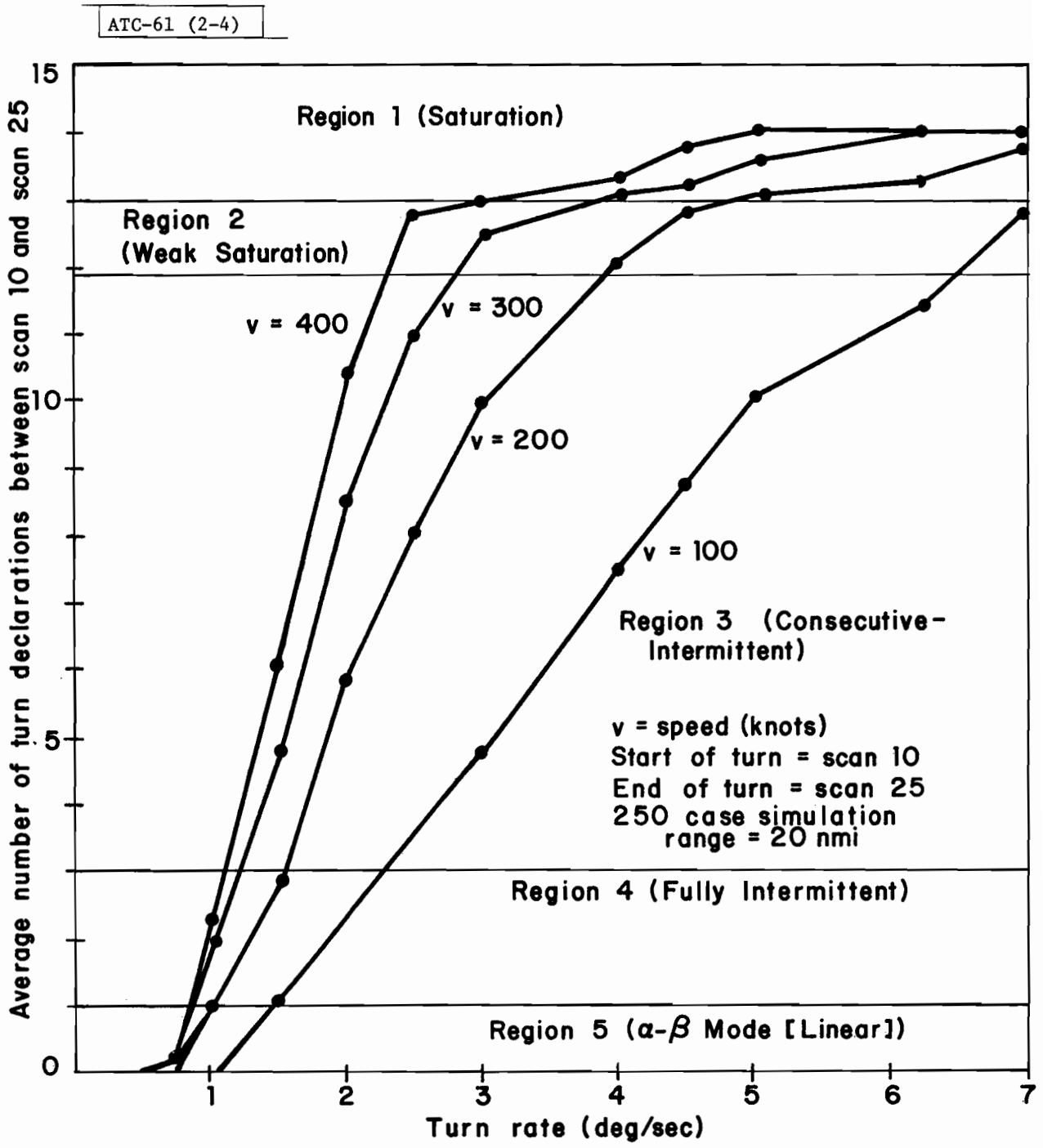

Fig. 2-4. Tracker behavior modes (regions).

Region 3: Consecutive Intermittent Mode. During some portion of the turn, turn declaration occurs for two or more consecutive scans.

Region 4: Fully Intermittent Mode. A turn declaration is followed by one or more scans during which the turn detector is disabled (i. e., turns are not declared on consecutive scans).

Region 5: α-β Mode. The turn declaration mechanism is off during the duration of turn.

The subdivision indicated in Fig. 2-4 is idealized. There are borderline cases that are difficult to classify, e.g., a 100-knot trajectory, with a 4.5^{o}/sec turn rate, triggers the turn detector the first two scans of turn declaration. Subsequently, the turn declaration becomes intermittent. The 100-knot trajectory is classified as being a part of Region 3; although it is in saturation during the first two scans. This is an example of a degenerate case of Region 2.

Figures 2-5(a), 2-5(b), 2-5(c) and 2-5(d) illustrate heading error 'scatter' contained in Regions 1, 2, 3 and 5, respectively. Figure 2-1(b) is an example of operation in Region 4. Examples of triggering can be recognized where the heading error starts to decrease or is increasing at a noticeably smaller rate than during previous scans. For example, in Fig. 2-5(a), triggering occurs during scan 12. During scan 13, triggering occurs the second consecutive time, and an extra 15^{o} correction is made to the heading. An end-of-turn transient can also be observed. During scan 26 and for the majority of cases during scan 27, the turn declaration is triggered; although the turn has ended during scan 25. This is caused by the internal cross-track lag that has accumulated during the turn. It takes several scans to bring the internal cross-track lag below the threshold.

Figure 2-5(b) is a case of operating in the Weak Saturation region. The turn detector is in saturation to scan 20, where for a few cases, turn detection becomes intermittent. Figure 2-5(b) also illustrates that a 'tuning' of the heading error occurs for this particular case. 'Tuning' will be discussed in Section 2.3.1. Figure 2-5(c) is an example of operation in Region 3. In this case, the intermittent triggering causes the errors to fall into two areas: leading in heading, and lagging in heading. For cases where the heading error leads, two or more consecutive triggerings have occurred, and an extra 15^{o} correction is added to the heading estimate. For lagging cases, the trigger had been disabled during the previous scan.

For operating in the α-β region (Fig. 2-5(d)), the heading estimate attains a fixed lag. The cross-track offset, corresponding to this lag, causes the heading change during the scan (and the heading correction inserted by the linear-filter) to cancel each other. This cross-track offset is not suf-

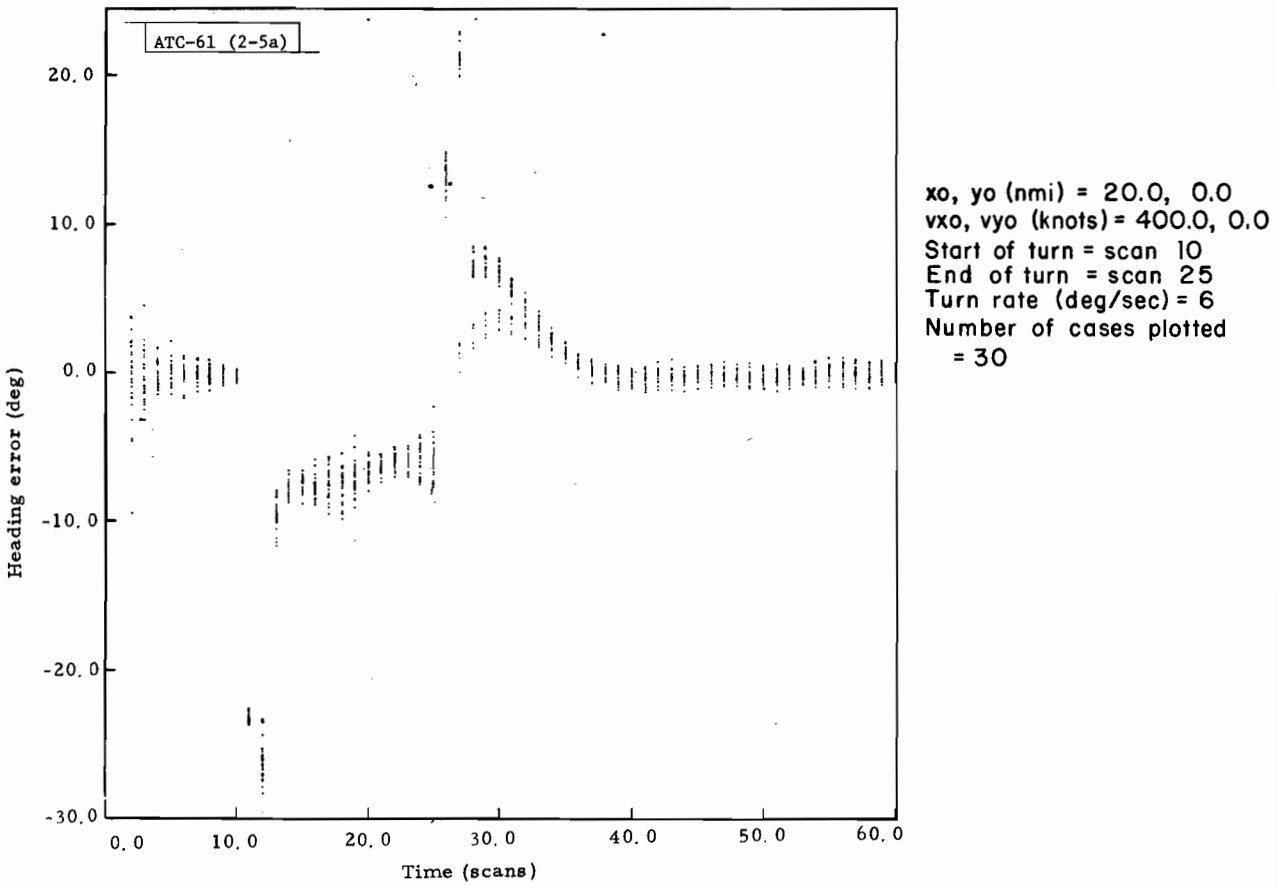

Fig. 2-5(a). Tracker dynamic heading performance in saturation mode (Region 1).

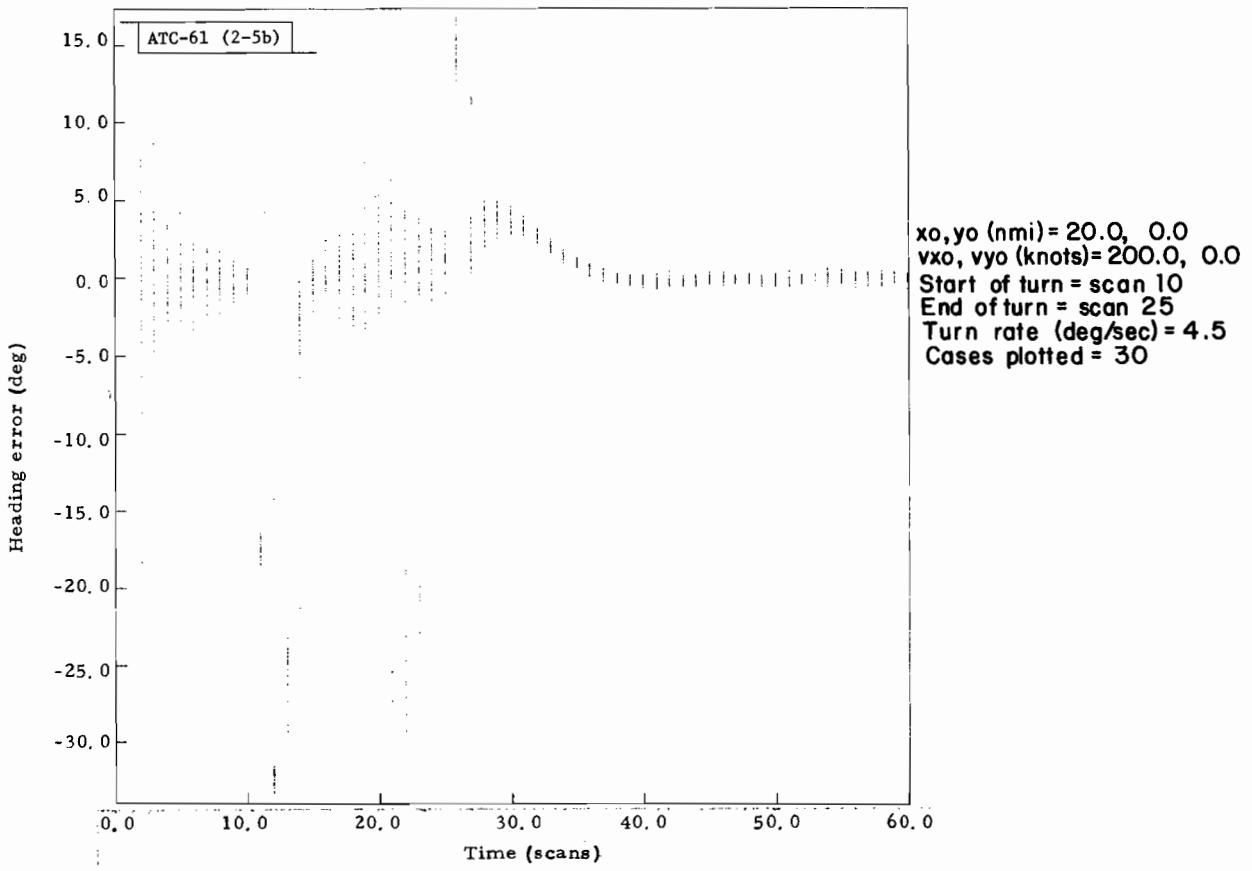

Fig. 2-5(b). Tracker dynamic heading performance in Weak Saturation Mode (Region 2).

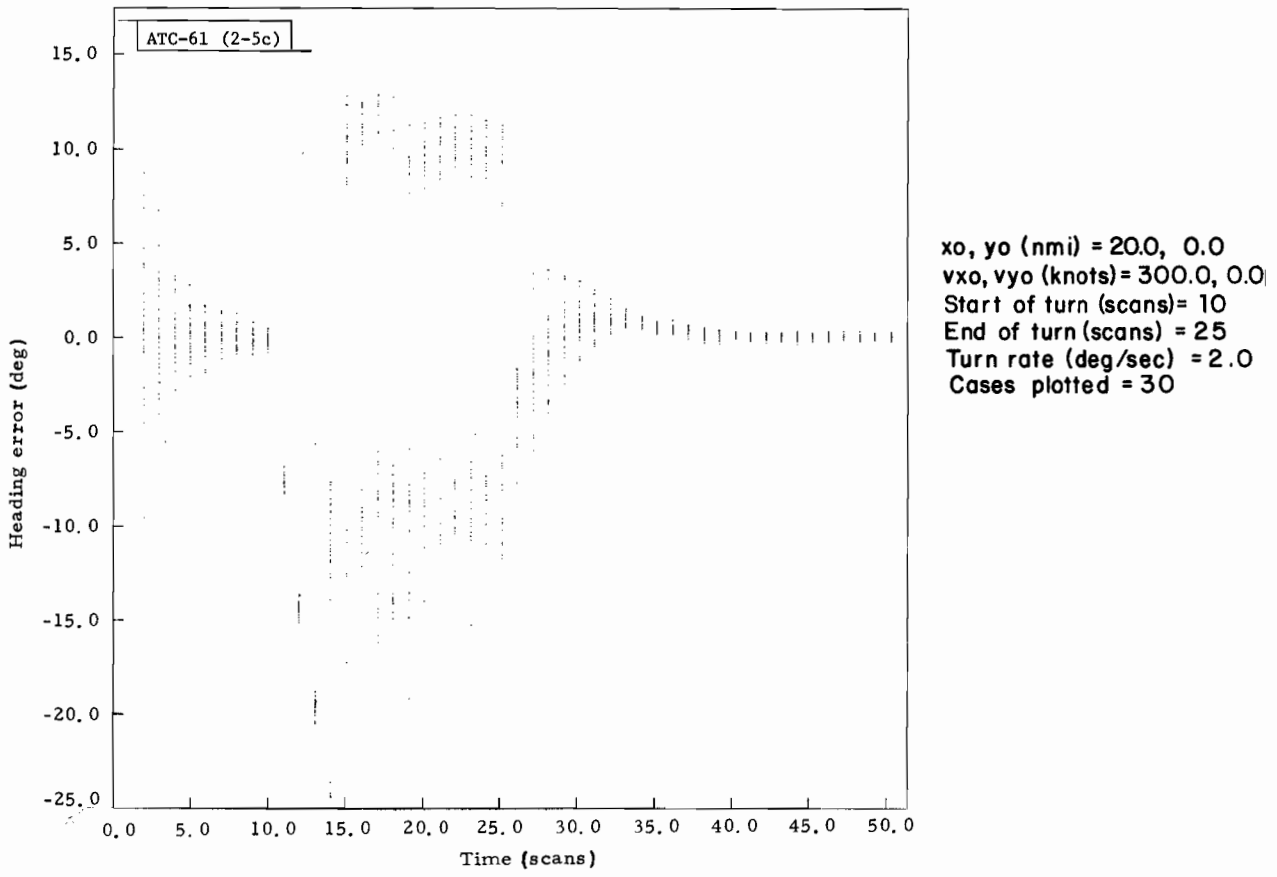

Fig. 2-5(c). Tracker dynamic heading performance in Consecutive Intermittent Mode (Region 3).

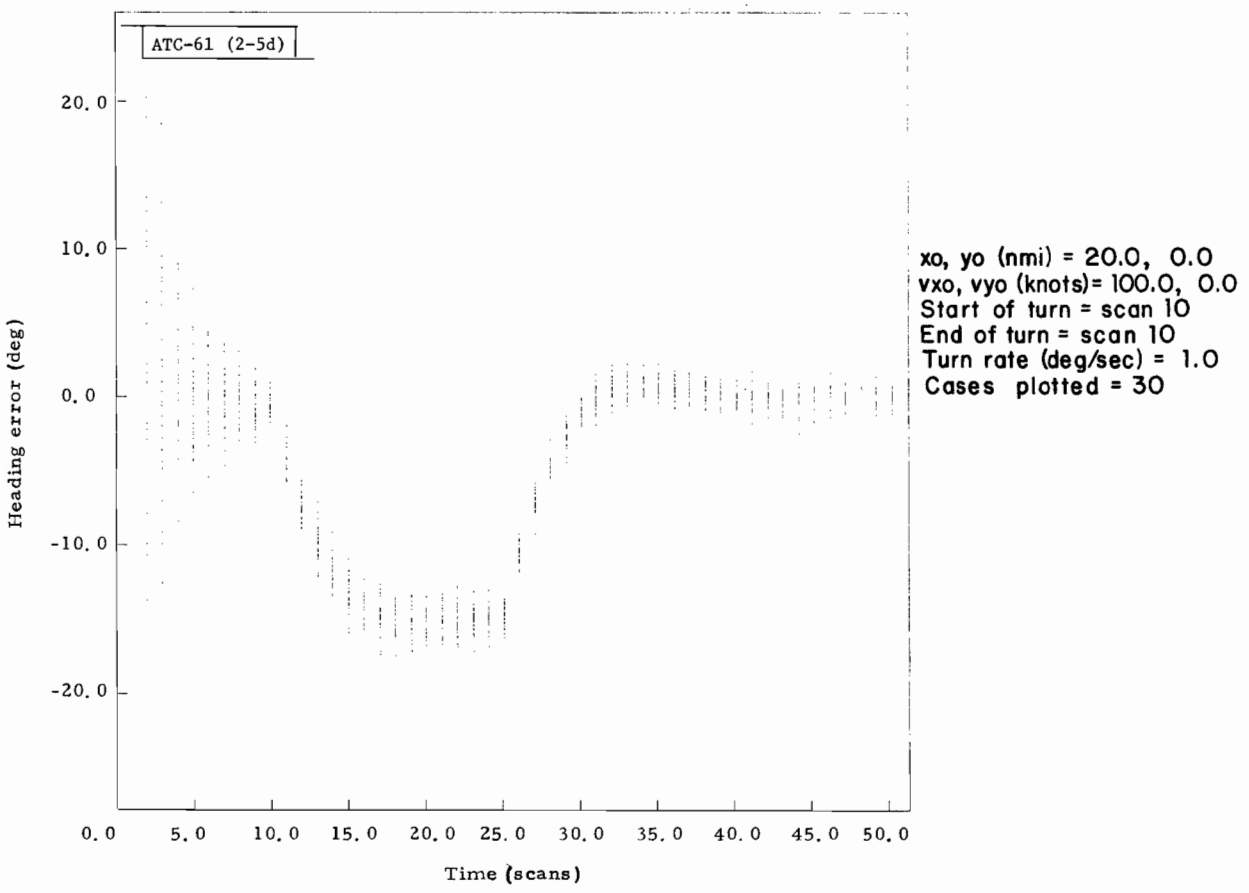

Fig. 2-5(d). Tracker dynamics heading for performance in Linear (α -β) Mode (Region 5).

ficiently large to trigger the threshold detector. For the fully intermittent case (Fig. 2-1(b)), the cross-track deviation required to cancel the heading change during a scan is slightly above the threshold, and as a result, triggering occurs. The triggering is fully intermittent in Fig. 2-1(b) because no cases appear where the extra 15° connection is made. The variations in tracker behavior previously described will help in understanding anomalies in tracker performance.

2.4 Tracker Heading Performance

2.4.1 Heading Error

Summarized root-mean-squared heading errors, as a function of turn rate for various fixed speeds at 20 nmi and at 40 nmi are indicated in Fig. 2-6. Each point plotted in Fig. 2-6 was obtained over the 250 cases for the reference turn (15 scans) illustrated in Fig. A-1. Note that near the 1.5°/sec turn rate, a leveling off occurs as turn declarations begin to take effect. The portion of the curves that tend to level off and, in some cases decrease, continues to approximately 5-6° sec. In the region of 6°/sec, the heading errors begin to increase at a more rapid rate. In this region, the half-angle error begins to exceed 20°. Because the half-angle correction is limited to 20°, a larger estimated heading offset is required in order that the α-β filter could cancel the excess turn rate. This larger heading offset is reflected in the increased error slope in the region of 6°/sec. For most higher speed aircraft, turn rates above 6°/sec are not practical; consequently, this region in Fig. 2-6 is of academic interest only.

The 200-knot case in Fig. 2-6(a) displays a local minimum at 4.5°/sec. (See Fig. 2-5(a).) It may be observed that, for some turn rates, the average heading offset during saturation is near zero. For this case, the extra 15° correction exactly cancels the estimated heading lag. For turn rates slightly above and below 4.5°/sec, the estimated heading would display a lag and a lead, respectively. The exact cancellation of estimated heading offset is defined as the 'tuning' of the tracker. Tuning also occurs at 4.5°/sec for the other speeds. Because the summary statistics represent accumulative rms error over the turn, the tuning is not readily apparent. For the 400-knot and 300-knot cases, the heading error lag prior to turn detection, and the out-of-turn transient shift the minimum away from 4.5°/sec. In the case of the slower aircraft, effects of tuning cannot be observed at all because, for those cases, turn detection is intermittent (Fig. 2-4). For turns in which the tracker operates in the saturation mode after a turn is declared, the heading error settles to a steady state value nearly independent of speed. Table 2-2 is a compilation of steady state errors for the saturation cases. It indicates the independent nature of the errors on speed. For low velocities and turn rates, this behavior cannot be observed because turn declaration cannot be sustained continuously. Lowering of the tracker threshold to correspond to data uncertainties used in this simulation would extend the saturation region into the low velocity and low turn rate area. Table 2-2 also indicates the tuning of the tracker described previously and confirms that it occurs between 4°/sec and 5°/sec.

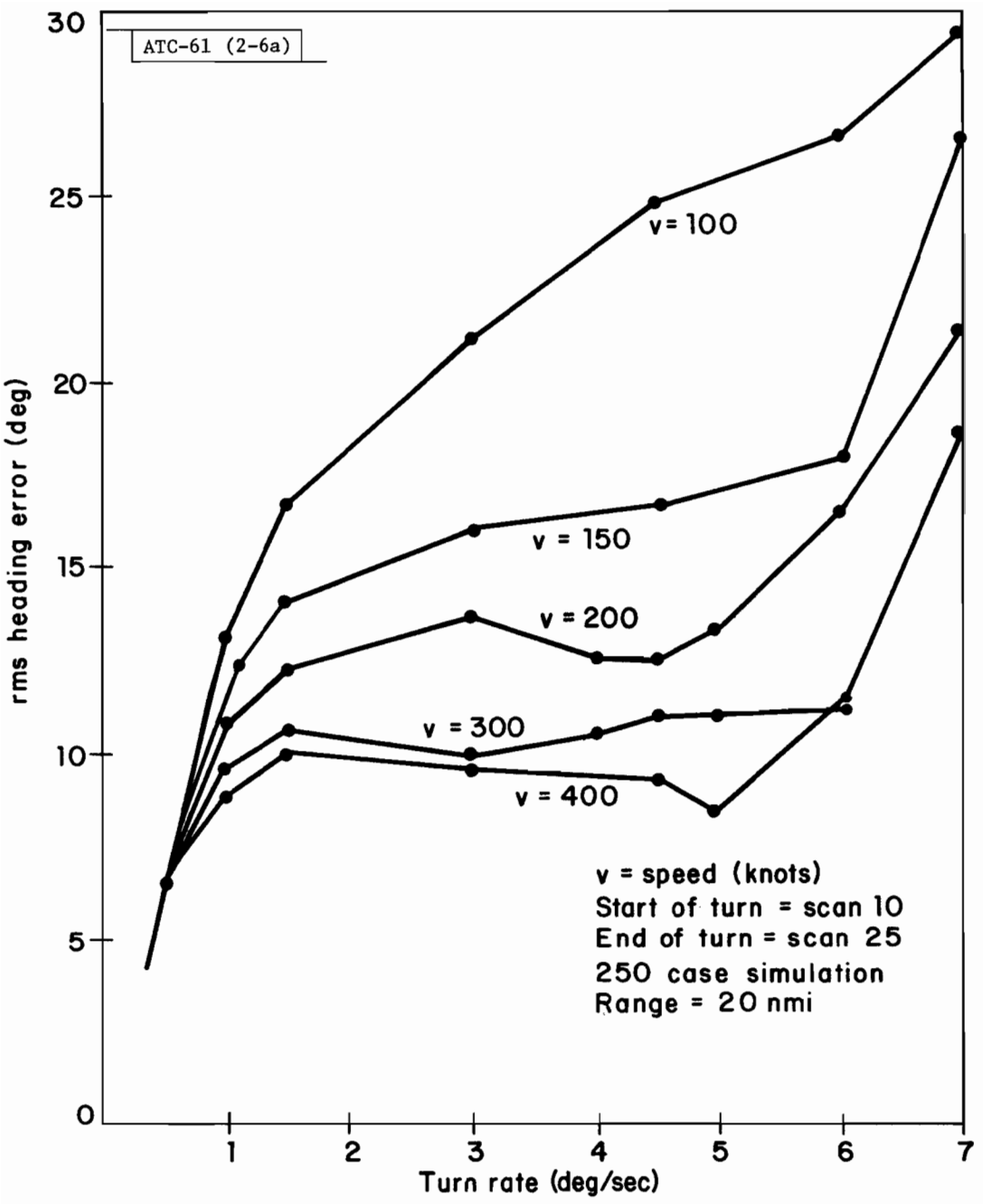

Fig. 2-6(a). Heading error vs turn rate (20 nmi).

For the cases illustrated in Fig. 2-6(a), Table 2-3 indicates the maximum rms heading error and (in parentheses) the number of scans of turn which occurred when the maximum error is achieved. For operation in the nonlinear region (at approximately the cases above the dotted line), the maximum error occurs one scan prior to turn detection or during the scan where turn detection begins. In the α-β region (at approximately the cases below the dotted line), the heading error builds up to a maximum value which corresponds to the steady state lag. In the low turn rate region (near 1^{o}/sec), the characteristic curves in Fig. 2-6(a) begin to merge. In this region the tracker is operating in the α-β mode. For an ideal measurement, heading is independent of speed in the linear tracker region, in view of the fact that speed affects only the relative scaling of the estimated trajectory. Because the heading error introduced by the turn is considerably greater than the data noise, the non-ideal case closely approximates the ideal cases. For very small turn rates, the performance characteristics again become speed dependent. This will be discussed in Section 3.0, which will include straight line performance.

TABLE 2-2. STEADY STATE rms HEADING ERRORS DURING SATURATION AT 20 nmi (deg)

Speed (knots)

Turn Rate (deg/sec)	100	150	200	300	400
7.0	22.0	20.3	18.3	18.1	17.5
6.0	*	6.4	6.0	6.0	6.5
5.0	*	*	1.4	1.5	1.9
4.5	*	*	1.7	1.7	1.4
4.0	*	*	1.5	1.4	2.8
3.0	*	*	*	6.3	6.2

*No saturation.

TABLE 2-3. MAXIMUM HEADING ERROR AT 20 nmi (deg)

Speed (knots)

Turn Rate (deg/sec)	100	150	200	300	400
7.0	53.3(3)	47.5(2)	37.0(2)	30.6(2)	30.5(2)
6.0	49.2(3)	42.4(2)	39.2(2)	26.3(2)	26.0(2)
5.0			35.3(2)	29.0(2)	21.7(2)
4.5	43.1(3)	32.0(2)	31.9(2)	30.0(2)	24.9(2)
4.0			28.5(2)	28.2(2)	24.9(2)
3.0	35.1(4)	29.1(3)	26.4(3)	21.4(2)	21.4(2)
1.5	22.1(7)	20.1(6)	18.5(5)	17.3(4)	14.7(3)
1.0	15.2(10)	15.0(9)	14.7(7)	13.9(5)	13.0(5)
0.5	7.8(10)	7.7(10)	7.6(10)	7.6(10)	7.6(5)

( ) Number of scans of turn at which maximum rms heading error occurred.

Figure 2-7 illustrates the dynamic behavior of the tracker for a 6°/sec turn rate at several speeds. The error profile in this figure exemplifies many of the phenomena in tracker performance mentioned earlier. Prior to turn detection, the tracker is operating in the α-β region, as indicated by the superimposed error curves during scans 10 and 11, and for lower velocities during scan 13. The curves peak out during a scan previous to turn detection or where some detection is beginning to occur. For the higher speed trajectories, turn detection occurs earlier and is sustained for the duration of the turn. Verifying Table 2-2, for higher velocities (200 to 400 knots), the heading errors settle to a steady state value independent of speed. The steady state heading offset is of the order of 6° for this turn rate, which indicates that the tracker is slightly past the tuning point. For the 100-knot case, turn detection is sustained through only scan 17 and does not reach steady state. Two scans (to scan 19) are required for the cross-track positional error to build up sufficiently to cause turn detection to resume. Out-of-turn transients occur for the 200-to 400-knot trajectories; this is caused by the cross-track positional lag that has built up during the turn. During scans 26 and 27, turn detection is sustained to bring the lag below the threshold.

At longer range, tracker performance will degrade during turns because the threshold increases with range, which further delays turn detection. (Refer to Table B-2 in Appendix B.) Figure 2-6(b) and Table 2-4 illustrate the heading error-profile at the 40-nmi range. The standard trajectory was used again, and Fig. 2-6(b) and Table 2-4 correspond to Fig. 2-6(a) and Table 2-2 for the 20-nmi case.

Tuning may be observed, as in the 20-nmi case, in the region between 4°/sec and 5°/sec. It is designated in Fig. 2-6(b) as a flattening or a slight decline in the curves. Table 2-4, which corresponds to Table 2-2, presents heading error that occur during saturation. For most of the cases in Table 2-4, saturation cannot be sustained for the duration of the turn, and the steady state saturation is never attained. Nevertheless, by comparison with Table 2-2, Table 2-4 indicates the important fact that tuning and steady state saturation performance are almost independent of speed and range (or threshold).

At 40 nmi (Fig. 2-6(b)), a generally poorer performance is observed when compared to the 20-nmi case, with the effect of range more pronounced for the lower-speed aircraft. Table 2-5 indicates the maximum rms heading error during turns at 40 nmi. In the region where the tracker is linear for both the 20-nmi and 40-nmi cases (at approximately the turn rates below the dotted line), the heading error is almost independent of range. (Compare Tables 2-3 and 2-5.) In the nonlinear region, the heading error in Table 2-5 indicates a degradation of performance caused by the greater delay in turn declaration for the 40-nmi case. Both Table 2-5 and Fig. 2-6(b) indicate that the linear tracker region is extended to a higher turn rate region.

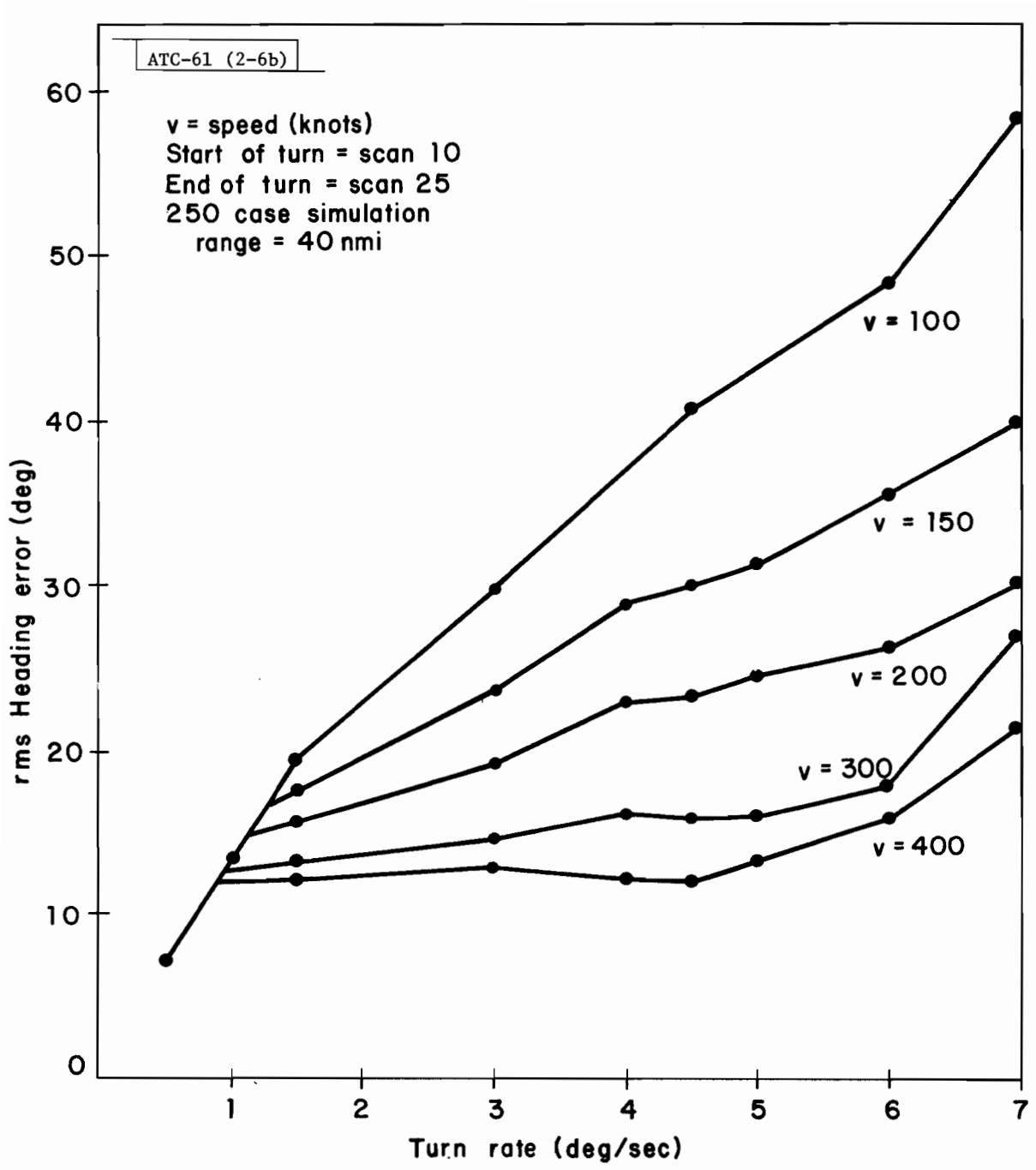

Fig. 2-6(b). Heading error vs turn rate (40 nmi).

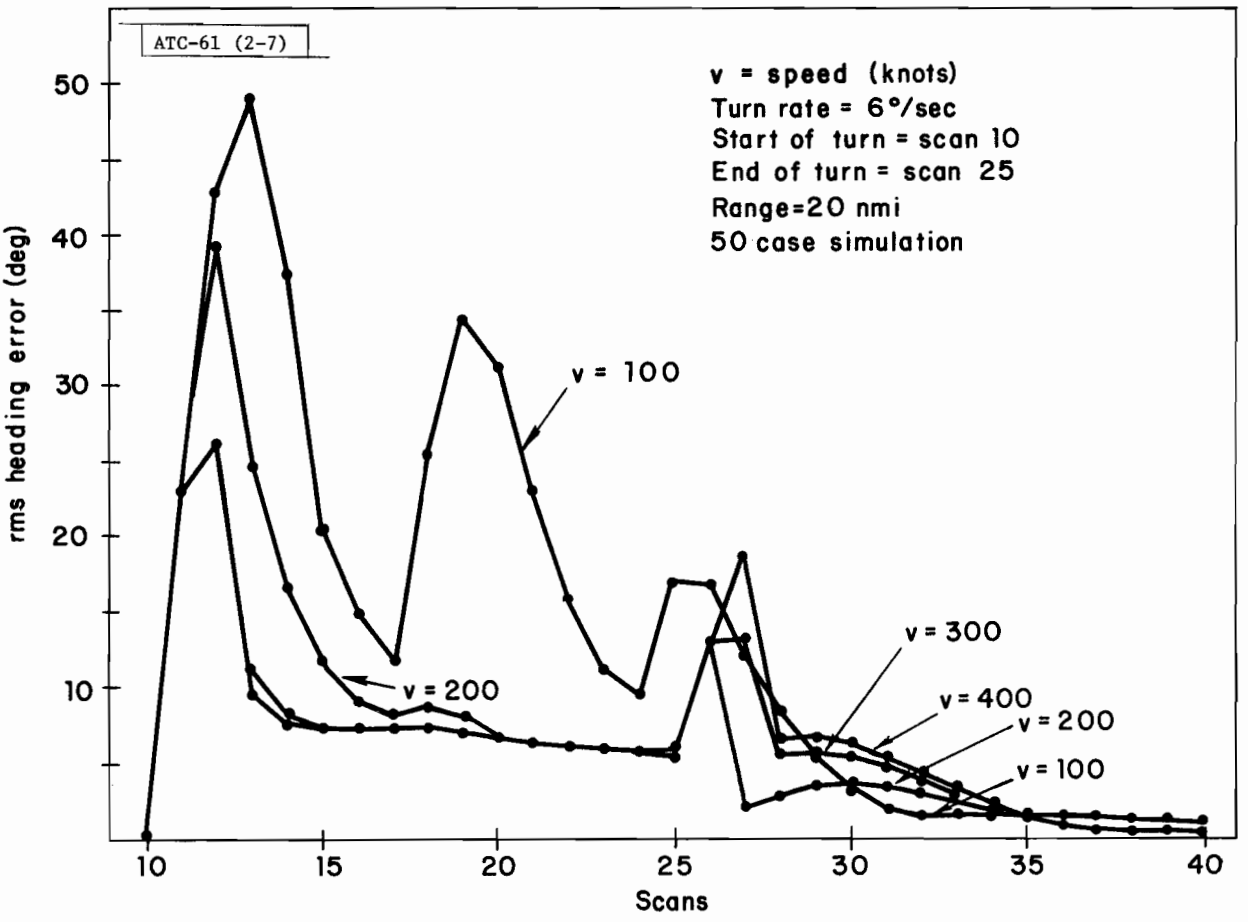

Fig. 2-7. Heading error vs scan (6.0°/sec, 20 nmi).

TABLE 2-4. STEADY STATE rms HEADING ERRORS (deg) DURING SATURATION AT 40 nmi

Speed (knots)

Turn Rate (deg/sec)	100	150	200	300	400
7.0	*	*	22.8	20.9	18.8
6.0			11.2	6.5	6.2
5.0			4.2	3.4	2.9
4.5			2.4	2.5	2.3
4.0			*	3.3	3.7
3.0	*	*	*	*	6.3

*No saturation.

TABLE 2-5. MAXIMUM HEADING ERROR (deg) AT 40 nmi

Speed (knots)

Turn Rate (deg/sec)	100	150	200	300	400
7.0	77.3(4)	64.8(3)	52.7(3)	47.1(2)	36.0(2)
6.0	67.2(4)	57.6(3)	48.3(3)	42.5(2)	37.5(2)
5.0	58.1(4)	48.9(3)	47.0(3)	35.6(2)	35.3(2)
4.5	54.8(5)	47.0(4)	42.7(3)	32.0(2)	32.0(2)
4.0	51.8(5)	43.8(4)	39.0(3)	31.4(3)	28.5(2)
3.0	42.6(6)	38.3(5)	33.4(4)	29.1(3)	26.7(3)
1.5	22.9(10)	22.5(8)	22.0(7)	20.5(6)	18.9(5)
1.0	15.5(10)	15.4(10)	15.2(10)	15.0(8)	14.7(7)
0.5	8.1(10)	7.9(10)	7.8(10)	7.7(10)	7.6(10)

( ) Number of scans of turn at which maximum rms heading error occurred.

2.4.2 Speed Error

Speed errors (250 cases summarized) vs turn rate for various speeds (for the reference turn of Fig. A-1) are indicated in Fig. 2-8(a). Generally, the maximum speed error occurs as a result of the end of turn transient. As a result, the rms value in Fig. 2-8(a) has been taken during the entire turn, including the end of turn transient to when the maximum cumulative rms is attained. Note that Fig. 2-8(a) is generally more linear regarding both the turn rate and speed as compared to the heading error profile in Fig. 2-6(a). The characteristic in Fig. 2-8(a) can be closely approximated by the following:

$$v_{rms}(S, W) = (S/100) \times v_{rms}(100, W)$$

where

$v_{rms}(S, W)$ = the cumulative rms error for the 100-knot case (Fig. 2-8(a))
S = speed (knots)
W = turn rate (deg/sec)

The effects of tuning and intermittent turn declaration, which greatly affect heading performance, are not apparent in the speed error profile. Several factors contribute to this characteristic.

(a) Heading corrections indirectly affect speed through the α-β filter. As a result, the intermittent nature of turn declaration appears in the speed errors in filtered form.

(b) Speed errors are affected by only the half-angle correction to the heading. The extra 15-degree correction is added to only the external velocity vector for IPC usage. As a result, during intermittent turn declaration, the effect of heading correction is further reduced. In view of the fact that tuning occurs as a proper balance between the half-angle correction and the extra 15-degree correction, it also does not affect the speed performance.

Figure 2-8(b) is a summarized heading error profile at a 40-nmi range. The behavior of the 20-nmi and 40-nmi cases closely resemble each other. At low turn rates and speeds, turn detection is delayed by a greater amount for the larger range. As a result, the value of the lag in speed, prior to turn detection, increases which is indicated by a slight upward shift of the curves in Fig. 2-8(b) for low turn rates as compared to Fig. 2-8(a). At 100 knots and 7°/sec, the speed lag previous to turn detection dominates the end of turn transient. This is illustrated as an increase in error in Fig. 2-8(b) for the 100-knot case.

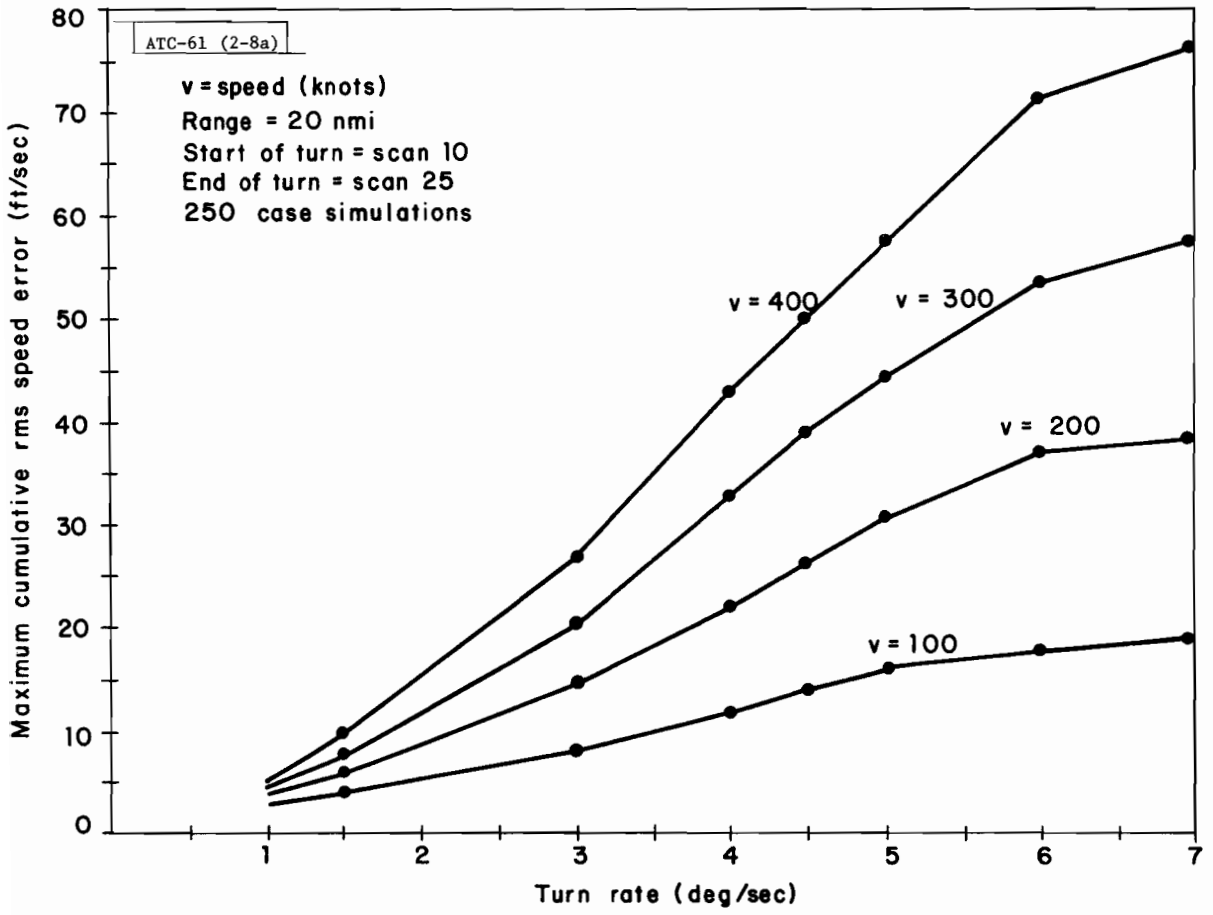

Fig. 2-8(a). Speed error (cumulative maximum) vs turn rate (20 nmi).

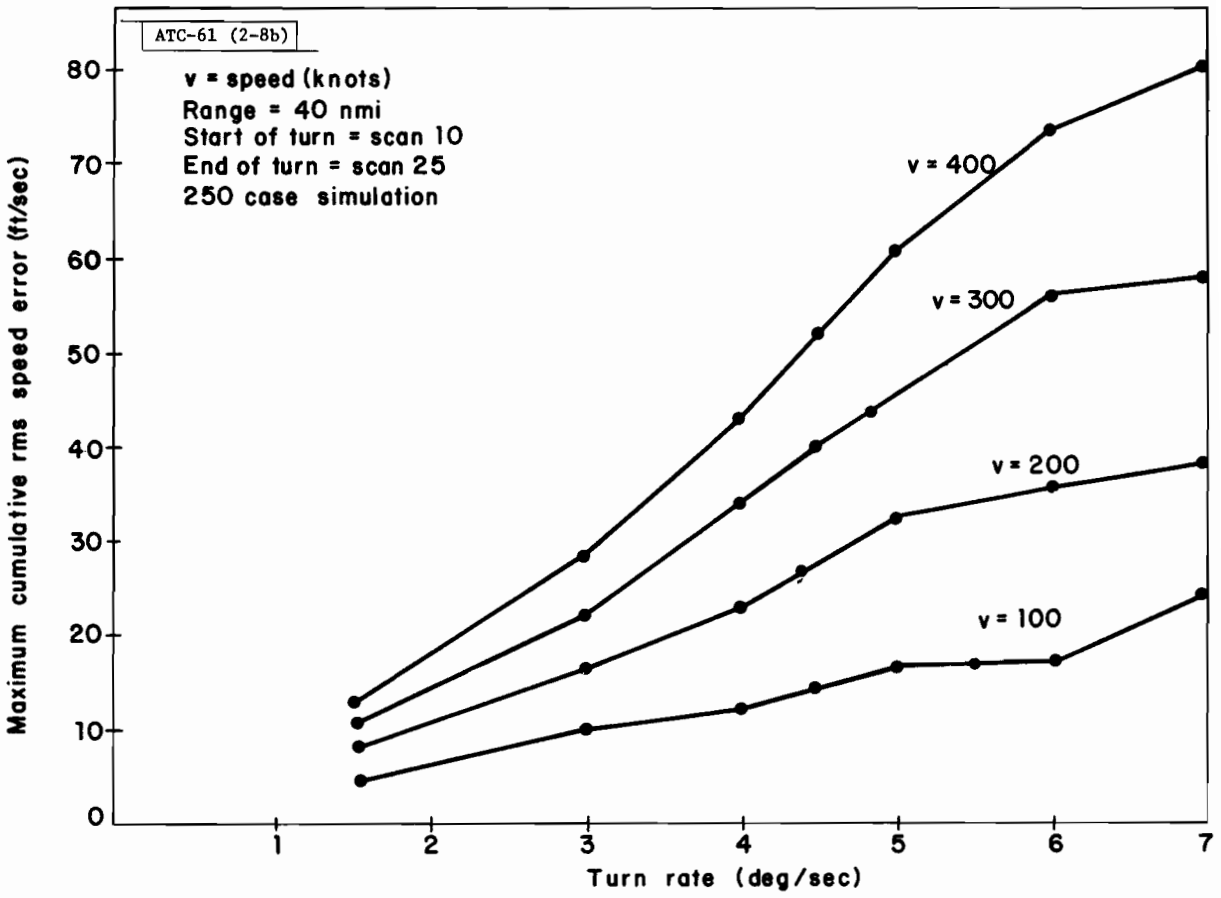

Fig. 2-8(b). Speed error (cumulative maximum) vs turn rate (40 nmi).

Figure 2-9(a) illustrates the dynamic speed behavior of a 300-knot aircraft turning at 2^{o}/sec (250-case simulation). Figure 2-9(a), which indicates typical speed errors, corresponds to Fig. 2-5(b) and illustrates that the intermittent turn declaration apparent in heading errors is largely filtered out in the speed error profile. Figure 2-9(b) illustrates a turn in which the turn detector is in saturation during the entire turn for most cases. Its error profile, similar to that in Fig. 2-9(a), corresponds to the dynamic heading errors indicates in Fig. 2-5(b).

Figures 2-9(a) and 2-9(b) illustrate several situations related to along-track error before and after turn declaration. Prior to turn declaration, estimated speed* is depicted as lagging. After a turn is declared, the estimated speed begins to lead the true speed. Fig. 2-10 illustrates the change in polarity of the speed error when a turn is detected. The along-track and cross-track errors, as the aircraft begins a turn, are indicated in Fig. 2-10(a). The positive along-track residue indicates to the α-β filter that the speed is too great; consequently, the filter reduces the speed for the new velocity estimate. Figure 2-10(b) is a diagram of the subsequent scan where it is assumed a turn is detected. The solid lines indicate the along-track and cross-track errors prior to turn declaration, and the dotted lines represent the errors after the turn is declared. The half-angle rotation of the estimated velocity vector introduces a positional lag along the new velocity estimate. This along-track lag, when filtered on subsequent scans, begins to increase the speed estimate, finally causing the estimated speed to lead the true speed.

An end-of-turn transient is evident in Fig. 2-9(b); this is related to the end-of-turn heading transient described in Section 2.4. The accumulated cross-track lag (during the turn) triggers the threshold during scan 26. This appears as a slight increase in speed error occurring one scan later.

Table 2-6 indicates the maximum rms speed errors and, in parentheses, the scan during which the errors occurred. In most cases, the maximum rms speed error occurs several scans after the turn has ended; this is caused by the sustained turn declaration after the turn has ended. It has been observed that the speed error increases with the angle of turn (Figs. 2-9(a) and 2-9(b) until it reaches a steady state offset. Speed error behavior is, thus, unlike heading error, which is large prior to a turn declaration; settling to a lower heading offset as the turn progresses. For shorter turns, the maximum speed error would decrease, and, as a result, the summarized speed error profile in Fig. 2-8(a) and 2-8(b) would improve.

Table 2-7 indicates the speed offset during saturation for the 20-nmi cases. The values in parentheses are percentages. Table 2-7 indicates that the percentage speed offset, as previously established for the heading offset, is independent of speed. For a 40-nmi case, Table 2-8 indicates that the speed offset (as the heading offset) is also independent of range.

*The polarity of speed error in Fig. 2-10 is in contrast to that in Fig. 2-9.

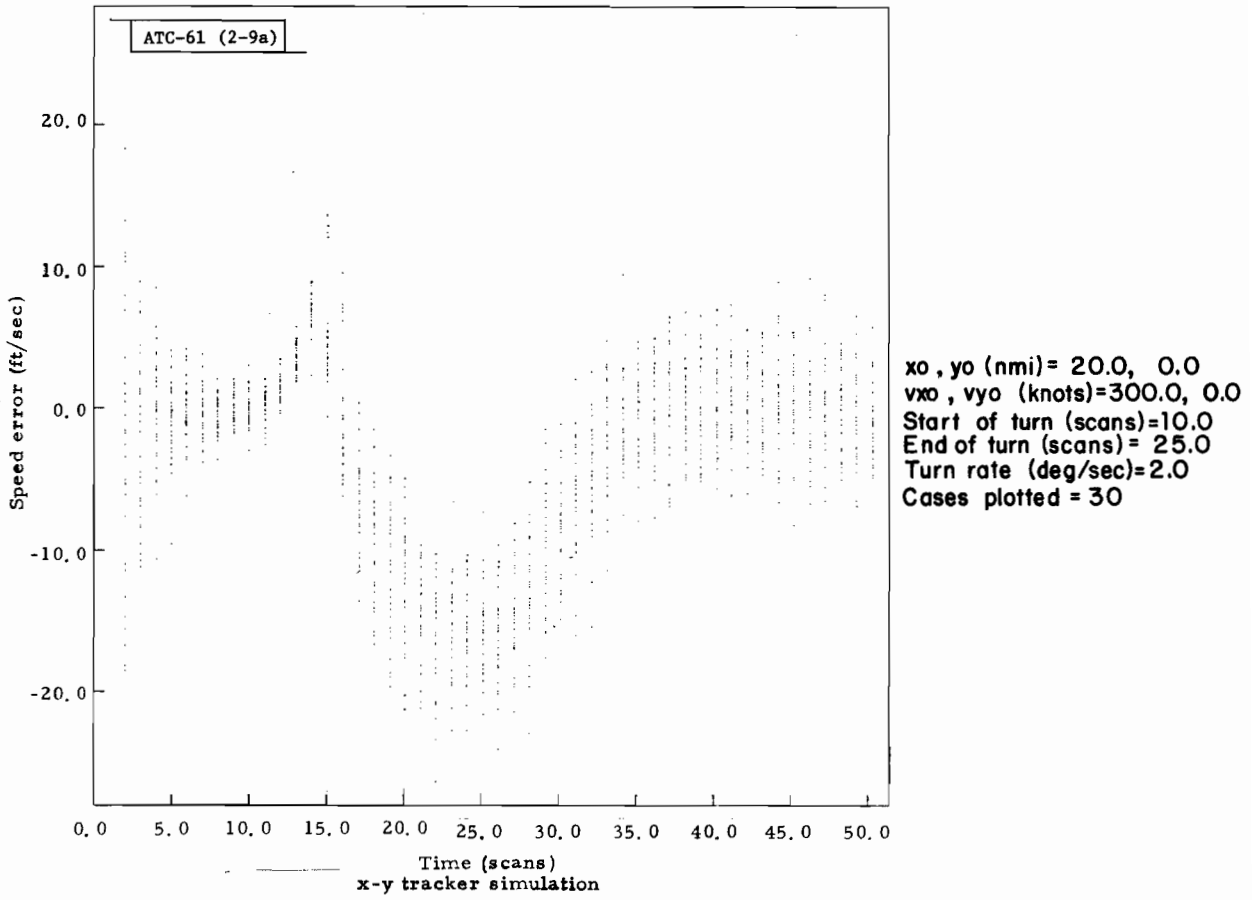

Fig. 2-9(a). Dynamic speed error vs scan (2.0°/sec, 20 nmi).

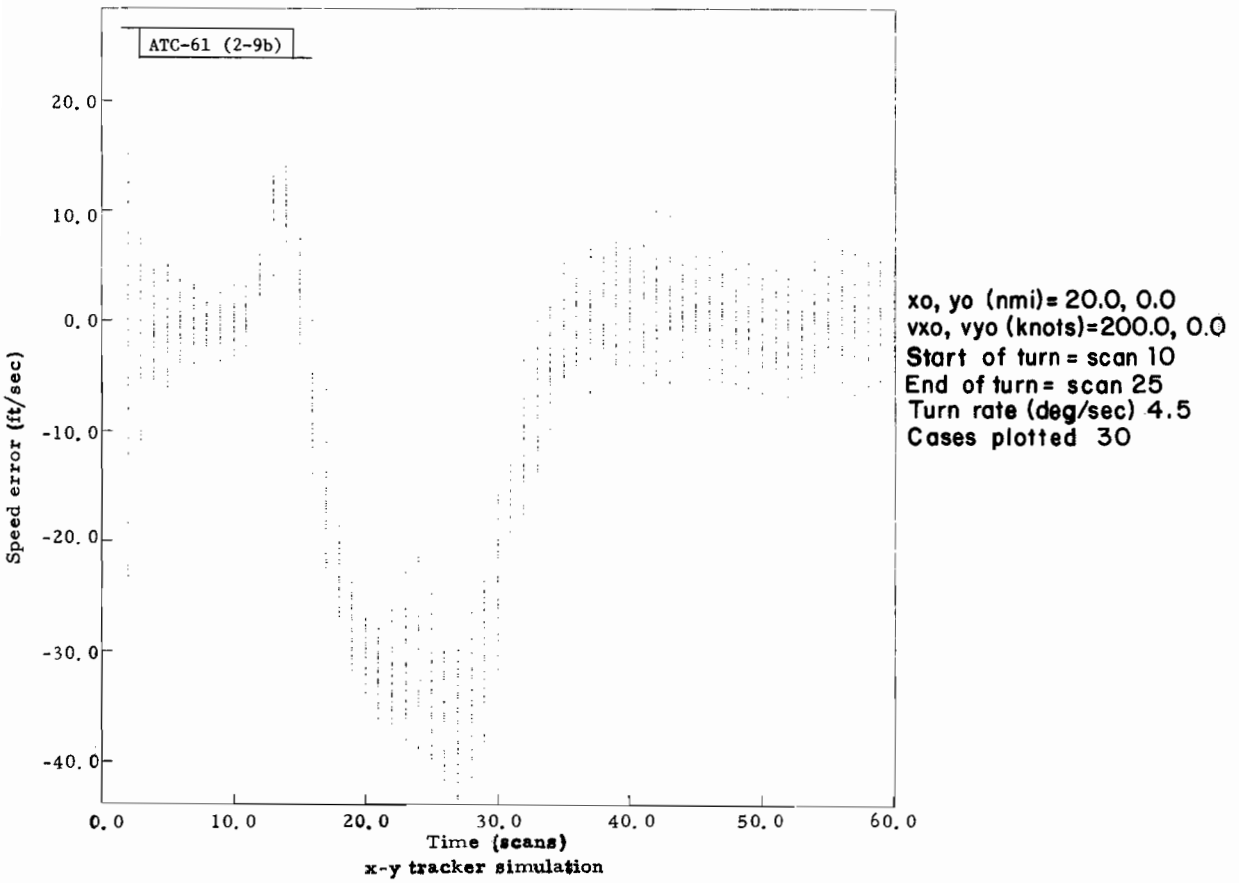

Fig. 2-9(b). Dynamic speed error vs scan (4.5°/sec, 20 nmi).

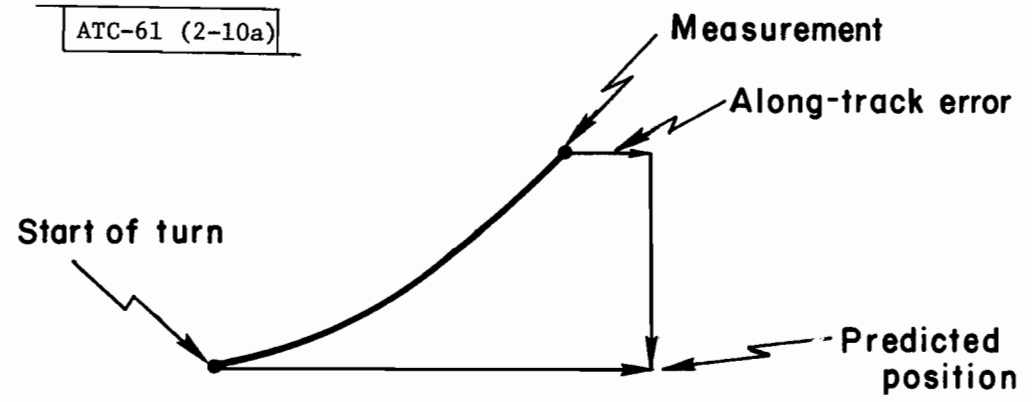

Fig. 2-10(a). Along-track error before turn declaration.

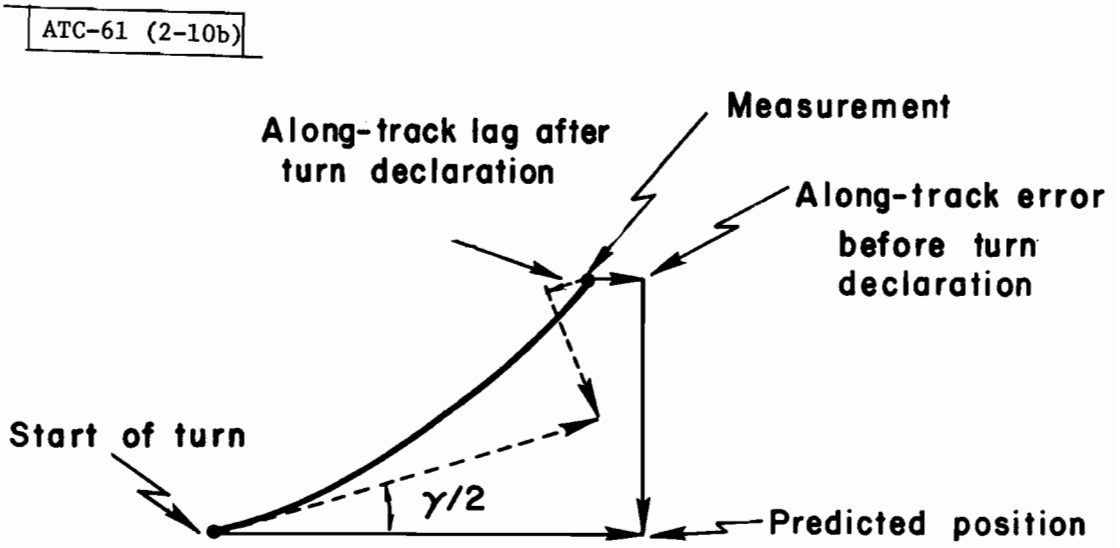

Fig. 2-10(b). Along-track error after turn declaration.

Turn Rate (deg/sec)	100	200	300	400
7.0	31.4(28)	65.6(28)	98.3(28)	131.0(28)
6.0	27.4(27)	55.1(27)	83.0(27)	108.5(27)
5.0	25.7(27)	43.3(27)	64.4(27)	85.3(27)
4.5	20.7(28)	36.7(27)	53.8(27)	71.4(27)
4.0	16.8(27)	30.3(27)	44.8(27)	59.7(27)
3.0	10.1(22)	18.5(21)	25.7(24)	34.8(26)
1.5	5.1(25)	8.2(26)	11.2(26)	14.2(26)
1.0	*	5.0(28)	6.3(28)	7.5(28)

*No saturation.

Speed (knots)

Turn Rate (deg/sec)	100	200	300	400
7.0	20.6	45.1(22.6)	69.0(23.0)	92.0(23.0)
6.0	24.7	48.8(24.4)	72.5(24.2)	94.6(23.7)
5.0	21.9	39.9(20.0)	59.0(20.0)	77.5(19.4)
4.5	16.0	33.1(16.6)	50.1(16.7)	66.1(16.5)
4.0	13.2	27.0(13.5)	42.7(14.2)	56.5(14.1)
3.0	10.1	18.5(9.2)	25.7(8.6)	34.1(8.5)

Speed (knots)

Turn Rate (deg/sec)	100	200	300	400
7.0	*	42.0(21.0)	65.7(21.9)	91.1(22.8)
6.0	*	49.1(24.5)	74.6(24.9)	98.5(24.7)
5.0	*	*	60.6(20.2)	79.9(20.0)
4.5	*	*	46.8(15.6)	67.9(17.0)
4.0	*	*	*	53.7(13.4)
3.0	*	*	*	*
1.5	*	*	*	*

*No saturation.

TABLE 2-7

STEADY STATE rms SPEED ERROR DURING 20 nmi (ft/sec)

2.4.3 Position Error

A. Projected Position Error

Tracker position estimates and velocity estimates are used to estimate aircraft position during several scans in the future. Although heading, speed, and position errors relative to the actual aircraft trajectory are important, the projected position error is an equally important measure of tracker performance. Projected position errors are calculated by using the actual and estimated velocity and position to project the aircraft position straight ahead 30 seconds into the future. A rectilinear projection is used by IPC even when turns are declared. The use of a 30-second projection time is somewhat arbitrary; however, reasonable approximation for other projection times can be obtained by scaling the results. From discussions of heading and speed performance, it is expected that the projected position performance will be dominated by heading errors. For example, using accumulated rms errors of heading and speed for a 200-knot aircraft; with a turn rate of 3^{o}/sec (see Figs. 2-6(a) and 2-8(a)):

Projected speed error = 15 ft/sec x 30 secs = 450 feet
Projected heading error = sin 20^{o} x 30 secs = 200 knots = 2050 feet

Position error is a less important contributor than speed and heading for the 30-second projection times.

Figure 2-11(a), corresponding to Figs. 2-6(a) and 2-8(a), illustrates the summarized rms projected position errors. In view of the fact that heading errors are the dominant contributor to the projected position performance, the conclusions pertaining to heading performance can be applied here. The characteristics of tuning, 20^{o} limit on the half-angle correction, and the effect of turn declaration in relation to heading performance (Fig. 2-6(a)) are evident here. Comparing the 200-knot aircraft in Figs. 2-6(a) and 2-11(a), a 'flattening' of error curves begins to occur in the region of 1.5^{o}/sec as turn declaration begins to take effect. In the region of 3^{o}/sec, the rms errors begin to decrease as tuning begins to take effect until a minimum is reached at 4.5^{o}/sec. Near 5.0^{o}/sec, the rms errors, affected by the 20-degree clamp on the half-angle correction, begin to increase rapidly. The projected position errors of Fig. 2-11(a) are related to the corresponding heading errors of Fig. 2-6(a) in Fig. 2-11(b). Note that the tuning effect (a) 3.0-4.5 deg/sec) is readily seen at aircraft velocities exceeding 100 knots.

The performance characteristics for projected position are reversed from those for heading in Fig. 2-6(a). The lower-speed aircraft, which exhibit a poorer heading behavior because of turn detection delays, nevertheless show an improved projected position profile. In Section 2.4, it was established that the maximum heading error is the accumulated heading lag previous to turn declaration. Table 2-9 corresponds to Tables 2-3 and 2-4, and is a compilation of maximum projected position errors for various speeds and turn rates. For short turns, the 'predetection' error would become more

dominant in the summary performance profile illustrated in Fig. 2-11(a) and, therefore, would cause it to degrade.

For turns in which turn declarations saturate after a turn is first declared, it has been determined that speed and heading errors approach a steady state offset. For heading, this offset is almost zero at a rate of 4.5^{o}/sec. Table 2-10 corresponds to Tables 2-2 and 2-5 and indicates the steady state (or near steady state) projected position offset during saturation. Because tuning occurs for heading only, the projected position error profile in Table 2-10 is dominated by the speed performance near the tuned condition. Speed errors shift the tuning point to 4^{o}/sec for the projected position offset. The values in parentheses in Table 2-10 are the normalized position errors pertaining to 100 knots and, as expected from prior discussion, are independent of speed.

Figure 2-12 is an example of the dynamic projected position error and is mainly comprised of the heading and speed errors indicated in Figs. 2-5(b) and 2-9(b). For this case, the heading offset is near the tuned condition (Fig. 2-5(b)); therefore, when the heading offset reaches steady state (scan 15), speed errors dominate the projected position error. This is evident by observing that the speed error profile (Fig. 2-9(b)), starting at scan 15, appears in a scaled down form in the projected position error profile (Fig. 2-12).

The results of Section 2.4.1 have indicated that heading performance, as a result of greater turn declaration delays, degrades with range. The projected position errors at a larger range reflect this degradation of heading. Figure 2-11(c) corresponds to Fig. 2-8(b) and illustrates the rms projected position error at 40 nmi. The effects of greater delay during turn detection and, in general, the more intermittent triggering during a turn, cause tuning to be disguised to a greater extent for the 40-nmi case. The 'flattening' and decrease of error with increasing turn rate is not as evident in Fig. 2-11(c) as for the shorter range in Fig. 2-11(a). For example, the tuning of the heading error for a speed of 200 knots, which occurs at 4.5^{o}/sec in Fig. 2-11(a), is not evident in Fig. 2-11(b).

Table 2-11 indicates the maximum rms projected position error at 40 nmi. As the summarized rms error profile of Fig. 2-11(b), this table reflects the increased heading lag previous to turn detection. The numbers in parentheses in Table 2-11 indicate the scan into the turn during which the maximum error occurs. The turn length used in the standard trajectory is 15 scans. In view of the fact that for many cases in Table 2-11 the maximum occurs early in the turn, the maximum projected position for shorter turns would become more dominant in the performance characteristics of Fig. 2-11(c) causing them to degrade.

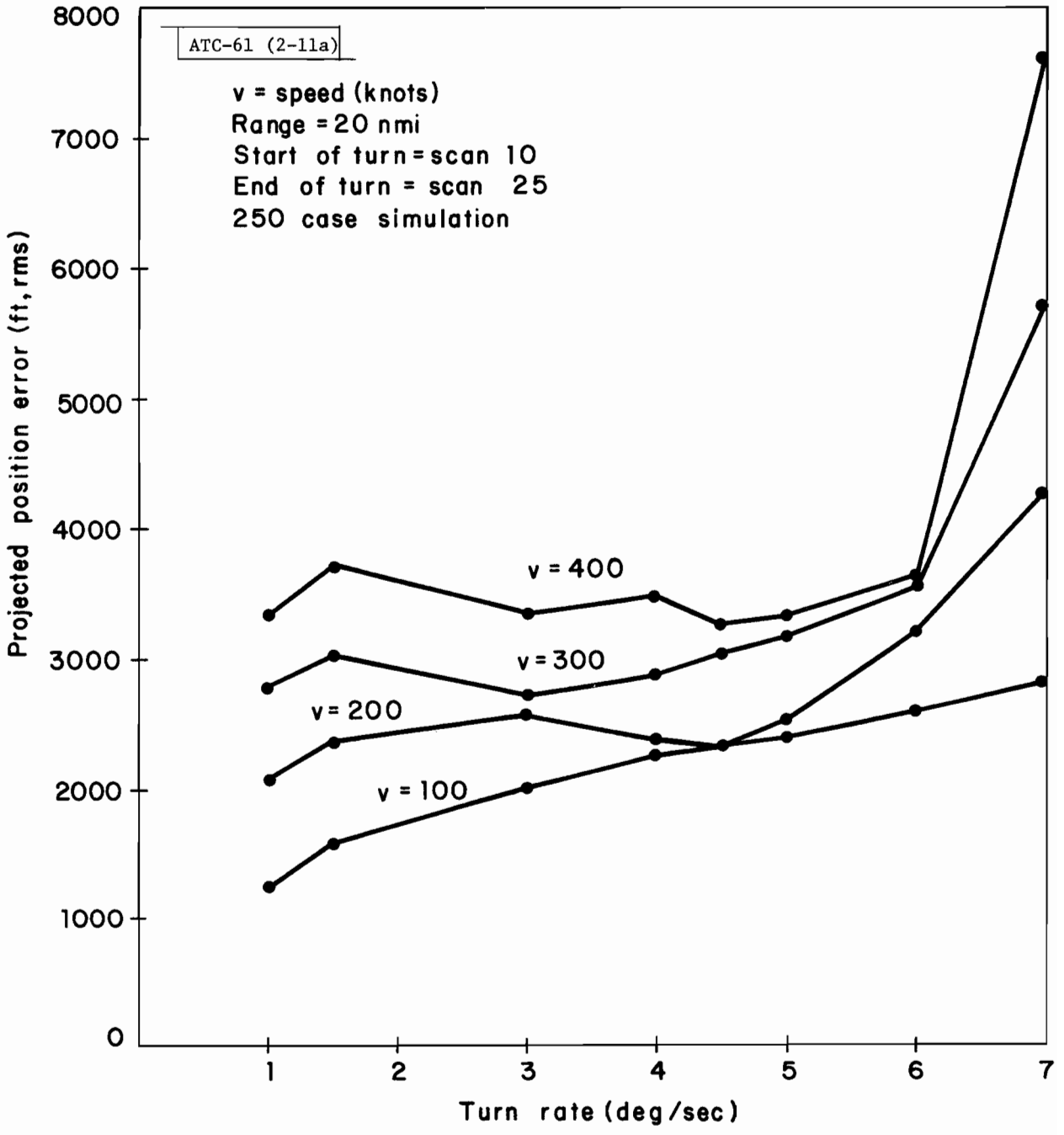

Fig. 2-11(a). Projected position error vs turn rate (20 nmi).

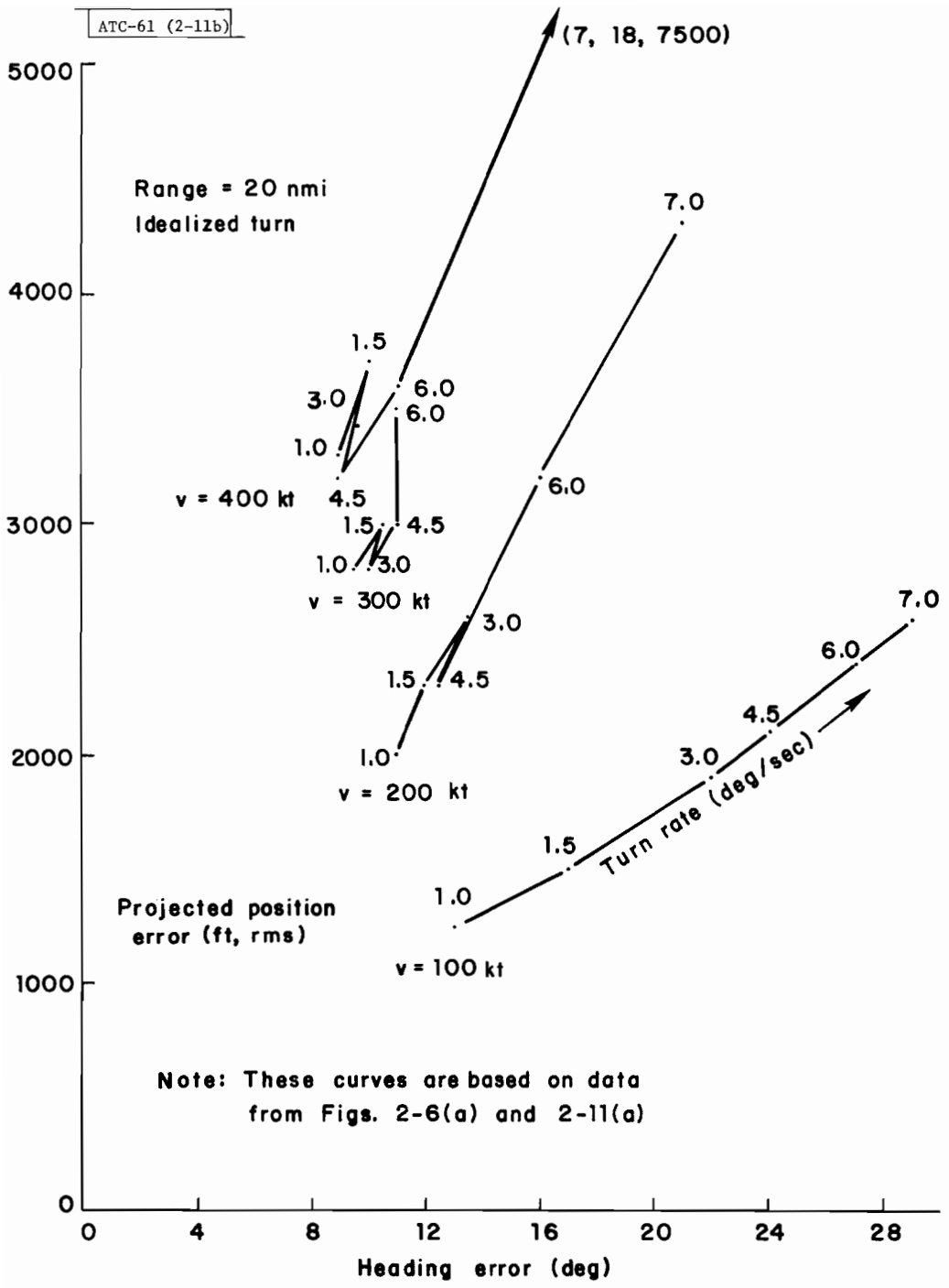

Fig. 2-11(b). Projected position error vs turn rate (40 nmi).

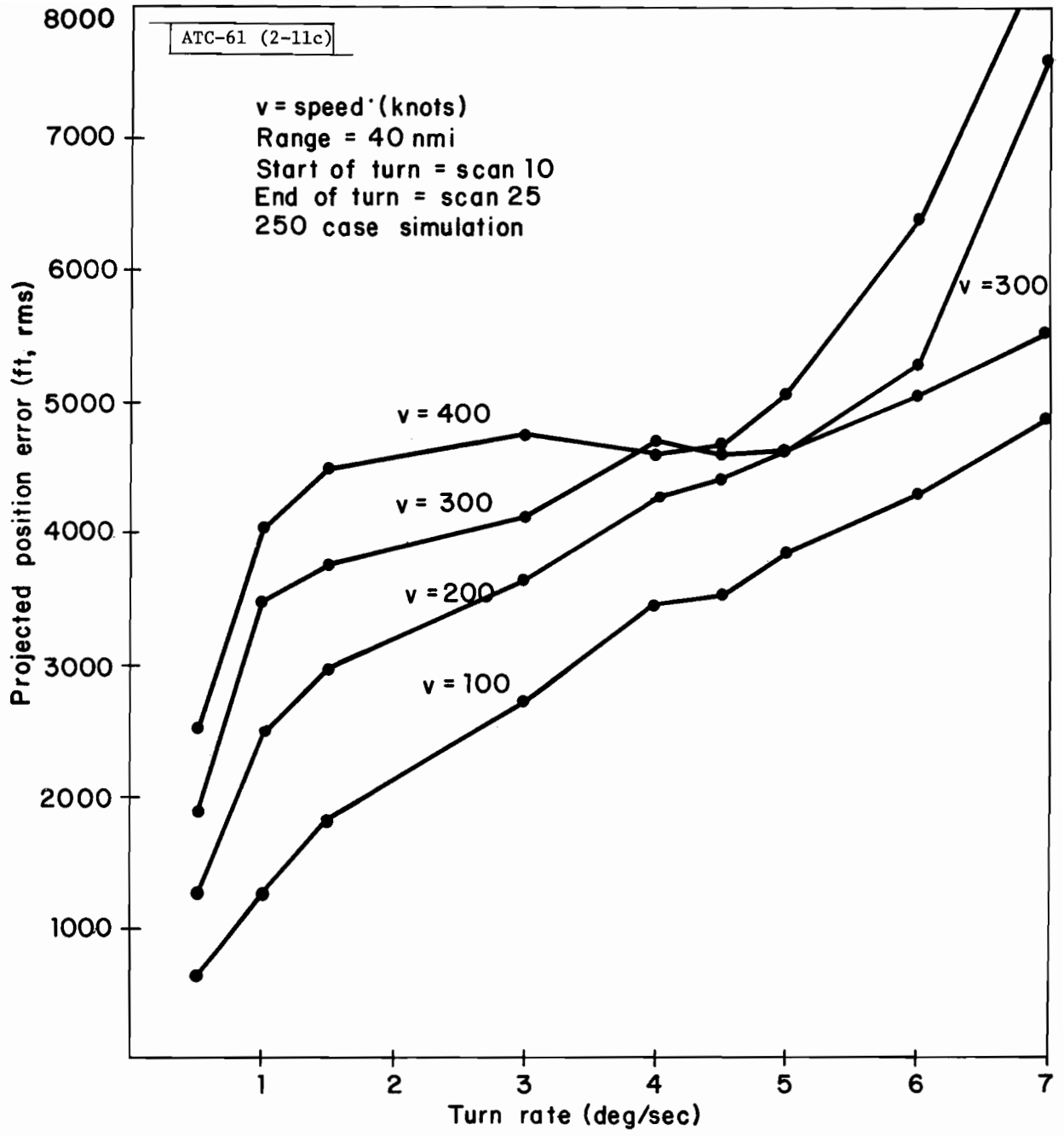

Fig. 2-11(c). Projected position error vs turn rate (40 nmi).

Speed (knots)

Turn Rate (deg/sec)	100	200	300	400
7.0	4597 (3)	6608 (2)	8364 (2)	11118 (2)
6.0	4301 (3)	6842 (2)	7234 (2)	9489 (2)
5.0	4111 (3)	6313 (2)	7841 (2)	8079 (2)
4.5	3837 (4)	5737 (2)	8051 (2)	8096 (3)
4.0	3481 (3)	5132 (2)	7630 (2)	9248 (3)
3.0	3086 (5)	4912 (3)	5806 (2)	7742 (2)
1.5	2046 (8)	3500 (6)	4685 (4)	5398 (3)
1.0	1418 (10)	2711 (7)	3736 (6)	4809 (5)

Speed (knots)

Turn Rate (deg/sec)	100	200	300	400
7.0	2205	4152 (2076)	6073 (2024)	8084 (2021)
6.0		2033 (1016)	2919 (973)	3835 (958)
5.0		1244 (622)	1807 (602)	2361 (590)
4.5		1134 (567)	1487 (495)	1935 (483)
4.0			1405 (467)	1832 (458)
3.0			1723 (574)	2367 (591)
1.5				

Speed (knots)

Turn Rate (deg/sec)	100	200	300	400
7.0	6142 (4)	9087 (3)	12507 (2)	13214 (2)
6.0	5713 (4)	8563 (3)	11271 (2)	13686 (2)
5.0	5013 (4)	8199 (3)	9553 (2)	12627 (2)
4.5	4745 (5)	7674 (3)	8631 (2)	11475 (2)
4.0	4489 (5)	6961 (3)	8950 (3)	10265 (2)
3.0	3724 (6)	6165 (4)	7915 (3)	9832 (3)
1.5	2112 (9)	4056 (7)	5537 (6)	6988 (5)
1.0	1453 (10)	2835 (10)	4214 (9)	5411 (7)
0.5	793 (10)	1469 (10)	2163 (10)	2862 (10)

TABLE 2-9

MAXIMUM PROJECTED POSITION ERROR AT 20 nmi (ft)

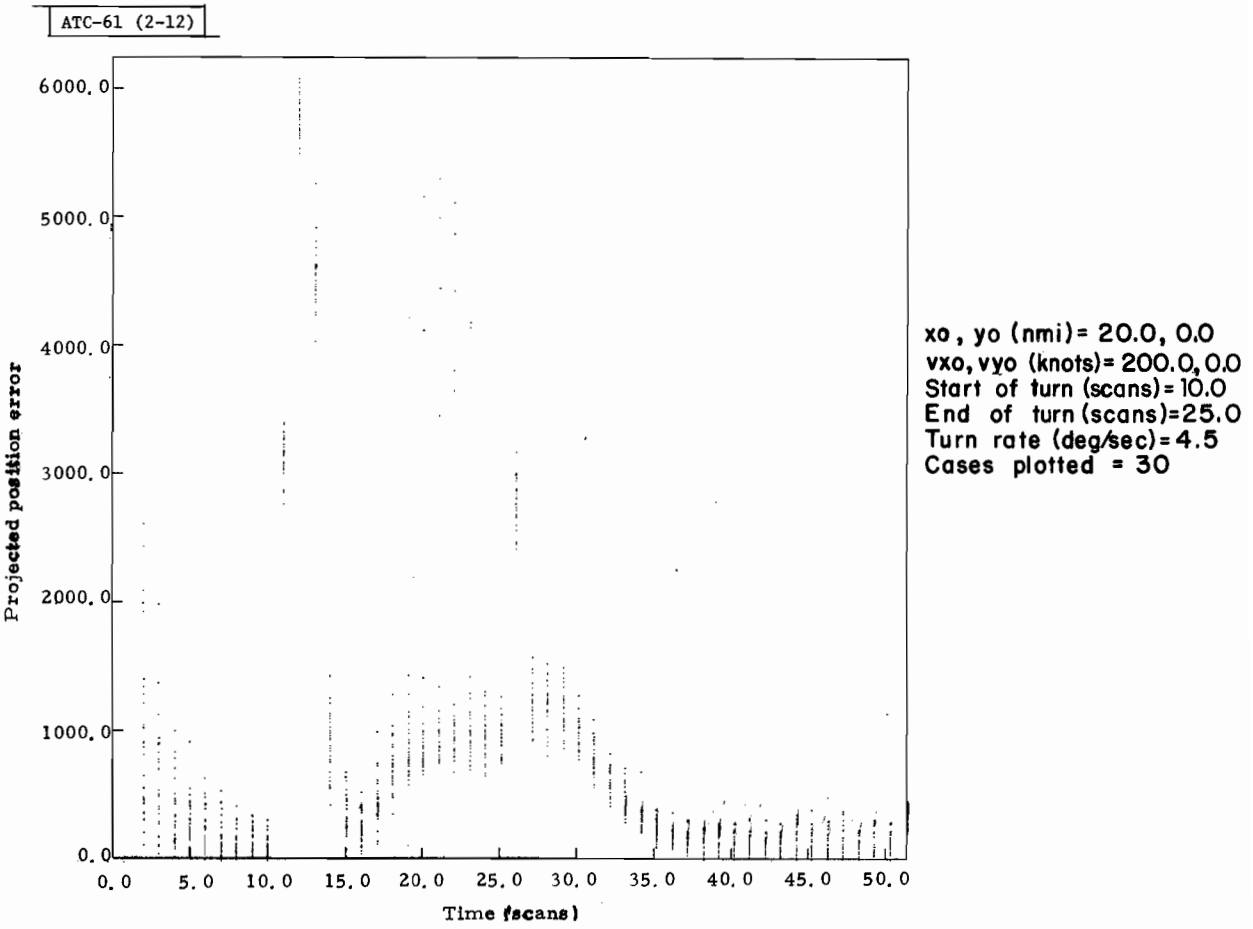

Fig. 2-12. Dynamic projected position error vs scan (4.5°/sec, 20 nmi).

B. Position Error

For purposes of this report, position error is defined as the projected position error for a projection time of 0 sec, and it is derived from the position estimates which are the output of the x-y tracker as a new data point is processed. Position error appears as a constant offset in the projected position independent of the projection time. Compared to heading and speed, the effect of position error upon projected position for reasonable projection times is secondary. Figure 2-13 illustrates the summary error profile and corresponds to the speed and heading error summaries previously presented. The behavior of the error profile in Fig. 2-13 is more linear than the heading error summary in Fig. 2-6. The reasons for this behavior are identical to those for the linearity of the speed error profile. Position estimates are not affected by the additional 15^{o} correction; however they are affected only indirectly by the half-angle correction through the α-β filter gains.

Table 2-12 indicates the maximum rms error during a turn. The numbers in the parentheses correspond to the scan into the turn during which the maximum error occurred. Note that the maximum position error for most cases is associated with the heading estimate lag previous to turn detection (compare Tables 2-3 and 2-12). The position error summary at 40 nmi is similar to the 20-nmi case, and because position errors have only a second-order effect on projected postion, it is not presented.

TABLE 2-12. MAXIMUM rms POSITION ERROR (ft) AT 20 nmi

Turn Rate (deg/sec)	Speed (knots) 100	200	300	400
7.0	289 (4)	482 (15)	708 (15)	939 (15)
6.0	268 (4)	432 (3)	517 (3)	684 (15)
5.0	249 (4)	383 (3)	502 (3)	576 (3)
4.5	232 (4)	350 (3)	494 (3)	567 (3)
4.0	213 (4)	315 (3)	463 (3)	575 (3)
3.0	194 (5)	301 (4)	356 (3)	470 (3)
1.5	145 (8)	222 (6)	288 (5)	331 (5)
1.0	117 (10)	185 (8)	238 (7)	298 (6)

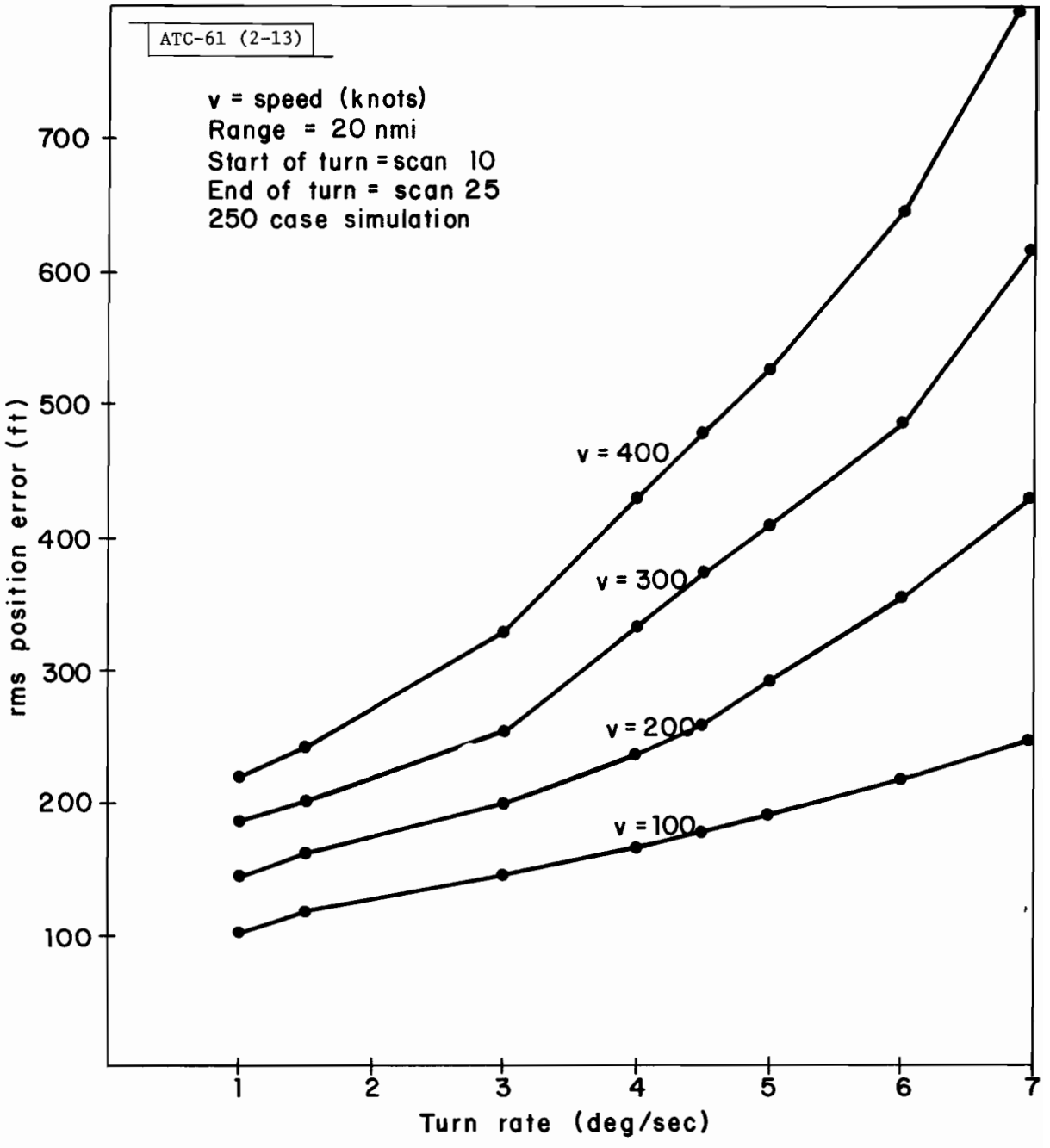

Fig. 2-13. Position error vs turn rate (20 nmi).

3.0 SIMULATED TRACKER PERFORMANCE USING RECONSTRUCTED TRAJECTORIES

In previous sections of this report, only ideal turns have been considered, i.e., as specified in Appendix A, Fig. A-1. An ideal trajectory was contructed that was comprised of straight line segments and circular turns, and it was assumed that linear accelerations were not present. Idealized turns are convenient because they allow an evaluation of the tracker under controlled conditions. For example, use of a turn, in which speed is not constant to present heading performance, would needlessly complicate the simulation.

In this section, turns reconstructed from real data are used in a simulation to supplement the ideal cases and to give some support to the results of Section 2.0. The trajectories are reconstructed from real data taken at DABSEF by using a standard third-order polynomial curve fitting technique. A window size of five scans is used in the curve fitting if, during any scan in the window, the real time IPC tracker declares a turn; otherwise a window size of seven scans is assumed. The curve fit trajectory is used to construct noisy tracks for the simulation. For the first case of the simulation, the actual data are processed by the tracker. For subsequent cases, Gaussian noise, as used in Section 2.0, is added to the reconstructed turn. Position, heading, and speed of the curve fit trajectory are used as standards against which position, heading, and speed obtained from the tracker estimates are compared.

3.1 Turning Track Performance

A common trajectory is a trajectory of an aircraft turning into the wind (Appendix A, Figs. A-2 and A-3). The wind distorts the turn and also causes the aircraft to lose ground speed (approximately 70 knots in the case in Appendix A.2). Figures 3-1, 3-2(a) and 3-2(b) illustrate the dynamic heading and speed profiles from a simulation using the turn as indicated in Fig. A-2. The maximum heading error in Fig. 3-1 is approximately 60°, which is consistent with the maximum rms heading error for a 100-knot aircraft turning at 6°/sec at a range of 40 nmi (Table 2-4). Note that the speed errors increase as a result of deceleration caused by the wind. Figure 3-2(b) illustrates the dynamic speed behavior for the ideal trajectory referred to in Section 2.0. Comparison of this error characteristic with the dynamic speed errors indicated in Fig. 3-2(a) indicates a significant increase in speed error for the decelerating aircraft. The deceleration also causes the speed estimate to lead* the true speed at the start of the turn, as contrasted with the lag that occurs prior to turn detection in the ideal case. The degra-

*The speed error polarities for Figs. 3-2(a) and 3-2(b) are reversed.

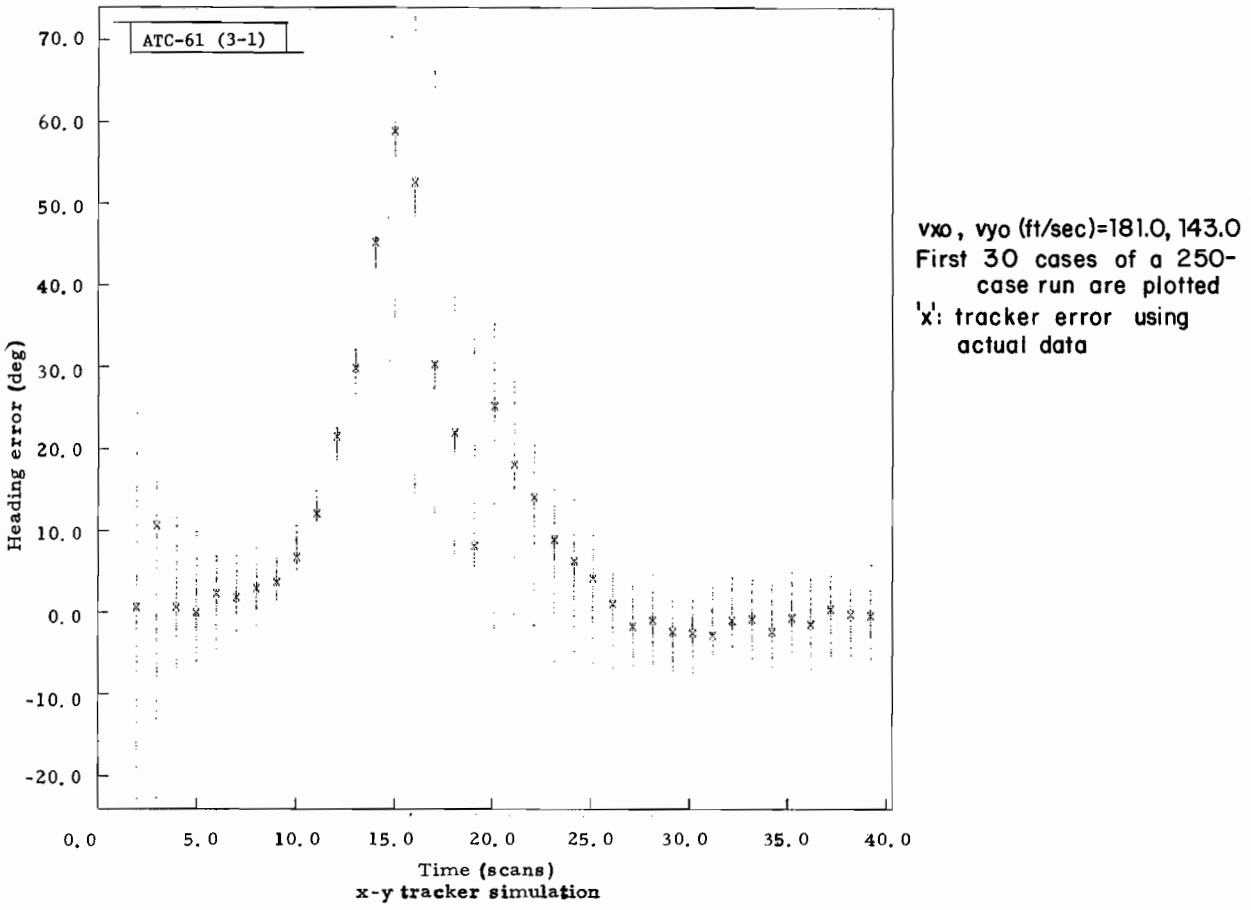

Fig. 3-1. Dynamic heading error vs scan for turn illustrated in Fig. A-2.

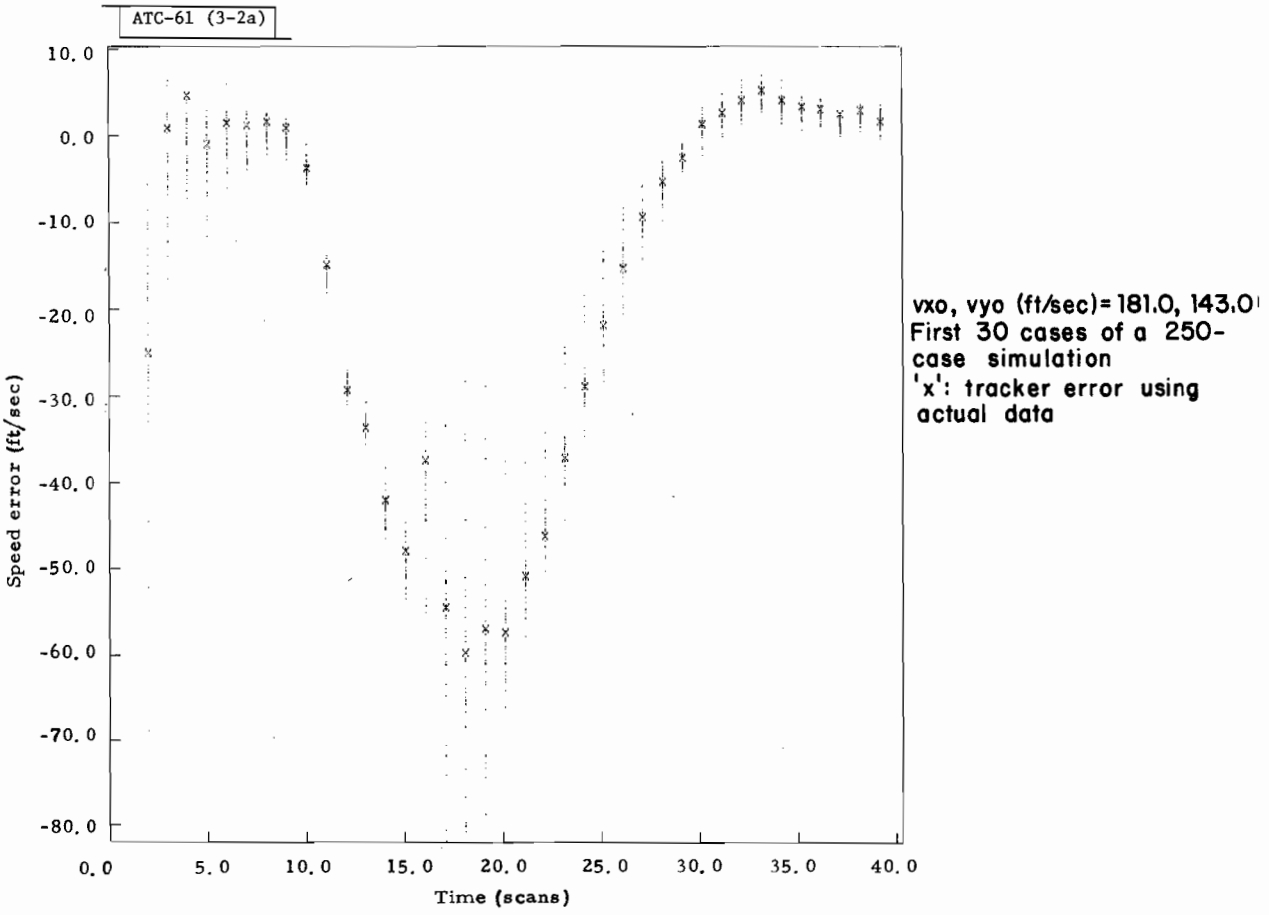

Fig. 3-2(a). Dynamic speed error vs scan for turn illustrated in Fig. A-2 (actual, in wind).

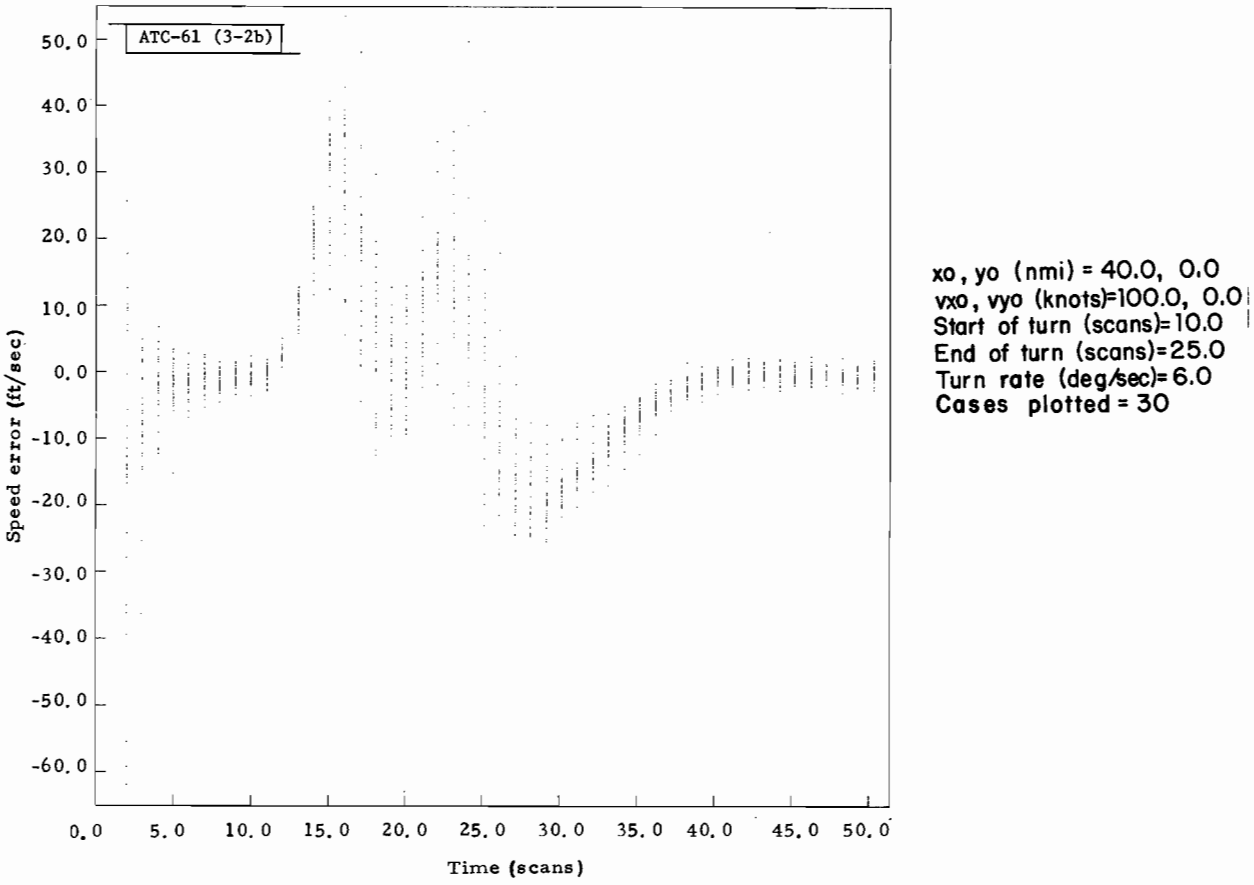

Fig. 3-2(b). Dynamic speed error vs scan for turn illustrated in Fig. A-1 (ideal turn).

dation in speed performance is expected for the decelerating aircraft, in view of the fact that position errors caused by speed changes are corrected only through the mechanism of the α - β filter.

A common maneuver during an IPC encounter is s-shaped. (See Appendix A, Fig. A-4.) In this case the aircraft temporarily changes direction in order to evade an approaching aircraft. Figures 3-3(a) and 3-3(b) illustrate typical dynamic heading and speed error profiles for the s-shaped maneuver (approximate turn rates of 3^{o}/sec). The maximum rms error during the first part of the maneuver (scan 16) is consistent with the heading error of the ideal 100-knot, 3^{o}/sec turn (Table 2-3). Because the turn starts abruptly for the ideal case, the turn is declared several scans earlier (Table 2-3). Consecutive turn detection at the end of the first portion of one s-maneuver (Fig. A-4, scans 18, 19 and 20) causes an overcorrection in heading. As a result, the counterclockwise turn starts with a sizeable heading lag. Consequently, early turn detection is possible (scan 21), although it cannot be sustained on subsequent scans. Deceleration during the clockwise turn and acceleration (as the trajectory transitions into the counterclockwise turn) 'cause' a lead followed by a lag in estimate speed (Fig. 3-3(b)). The speed error magnitudes are significantly larger than for an ideal (3^{o}/sec) turn (Table 2-6); nevertheless, they are still consistent with the heading errors. The s-maneuver is of interest because it is a maneuver that commonly occurs in IPC encounters. The estimated speed error that is associated with the speed change during this maneuver, although not excessive, causes the over-all tracker performance to degrade noticeably.

A final example of tracker performance in an actual situation is one that uses the reconstructed trajectory referred to in Appendix A, Figs. A-5, A-6 and A-7. A shallow turn occurs early in this trajectory. Near scan 25, the aircraft begins to turn until a rate of approximately 7^{o}/sec develops. Going into the turn, the aircraft decelerates to a speed of less than 50 knots, and it accelerates to its original speed coming out of the turn. As the aircraft completes the rapid turn, it changes direction; turning at an approximate rate of 4^{o}/sec. Near the end of the trajectory the aircraft changes direction again at a rate of 2.5^{o}/sec.

Figures 3-4 and 3-5 are the resulting dynamic error profiles of heading and speed from the simulation. The heading error profile indicates that the tracker operates in the linear region during the shallow turn. As the aircraft proceeds into the rapid turn, the associated speed reduction greatly impedes the ability of the tracker to detect the turn. The turn detection is delayed until scan 35, at which time a lag of more than 100 degrees has accumulated in the heading estimate. As the aircraft changes direction when coming out of the rapid turn (scan 38), the remaining heading lag appears as a lead for the clockwise turn. This situation delays turn detection for the 4^{o}/sec turn until scan 45.

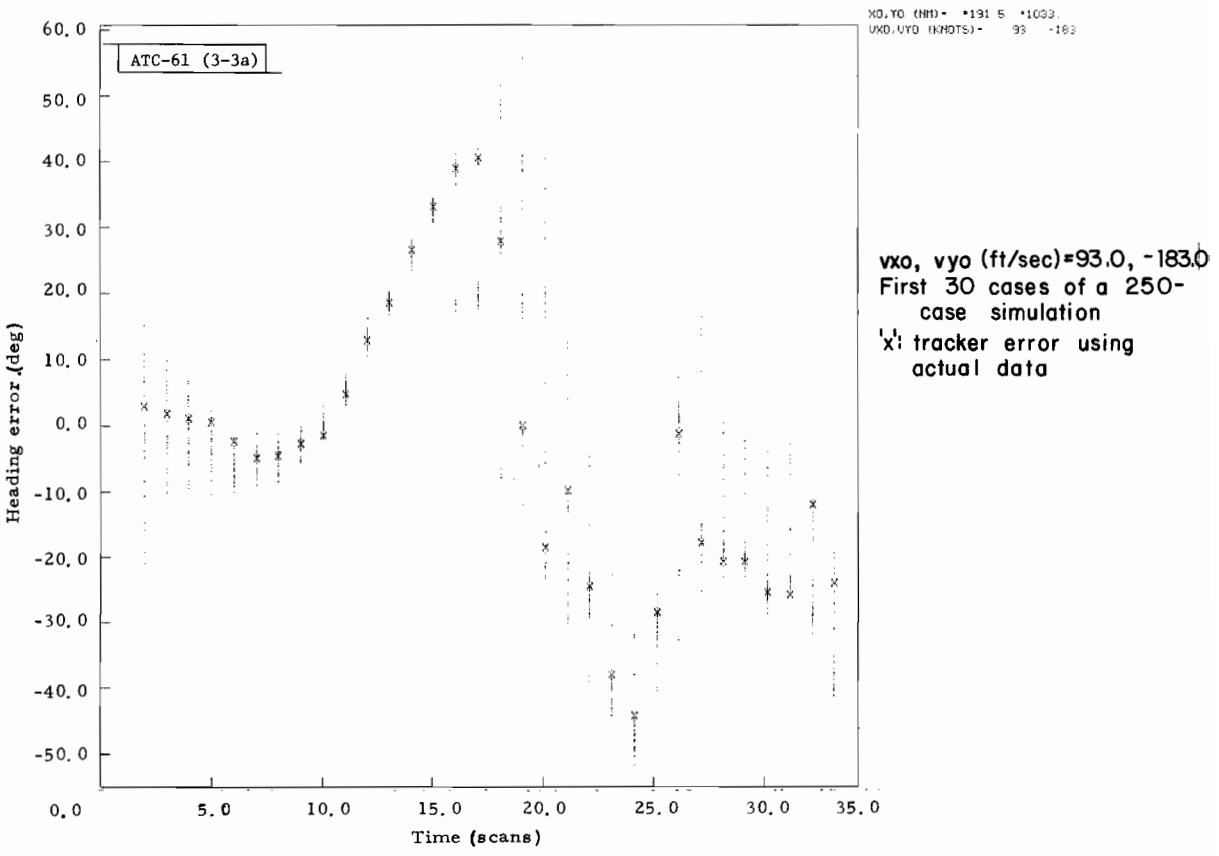

Fig. 3-3(a). Heading error vs scan for s-maneuver as illustrated in Fig. A-4.

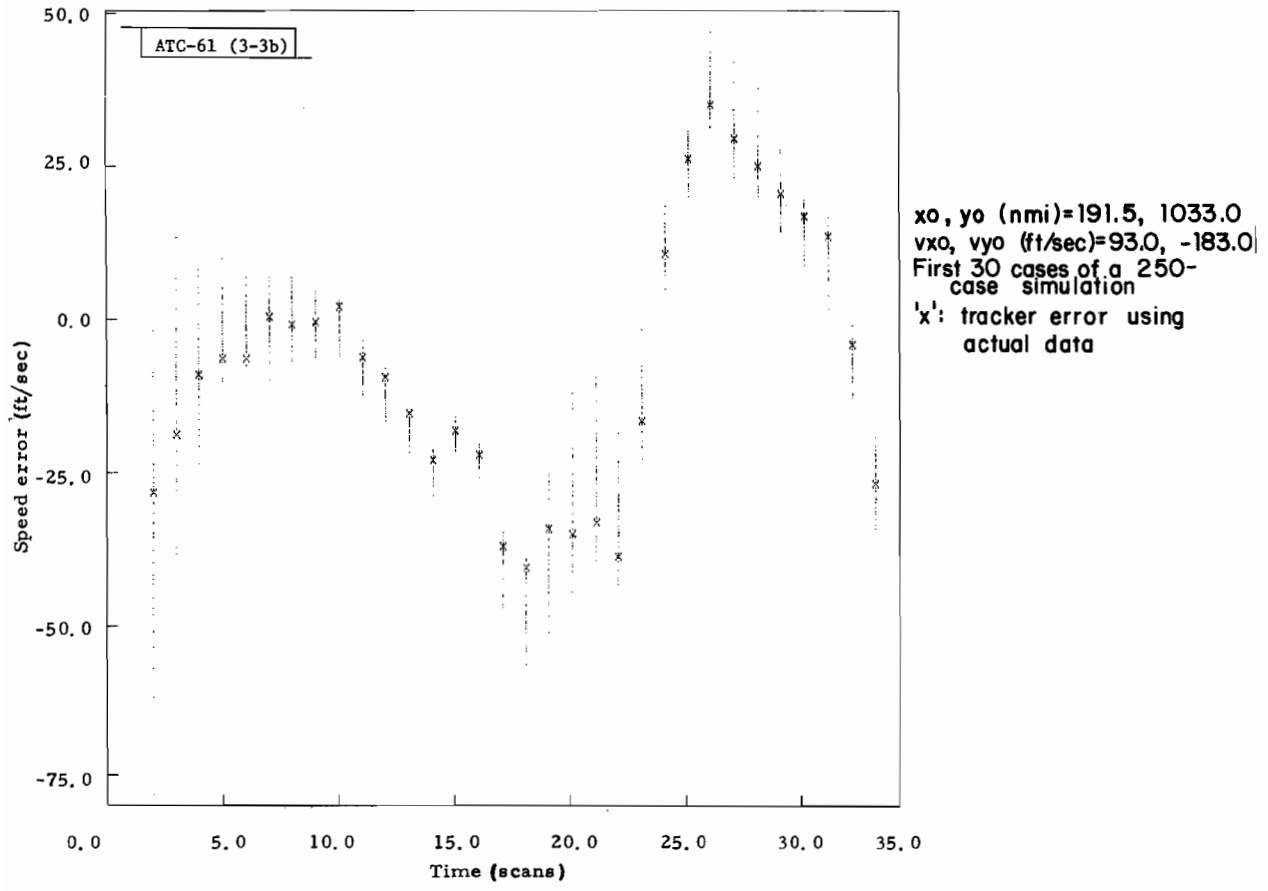

Fig. 3-3(b). Speed error vs scan for s-maneuver as illustrated in Fig. A-5.

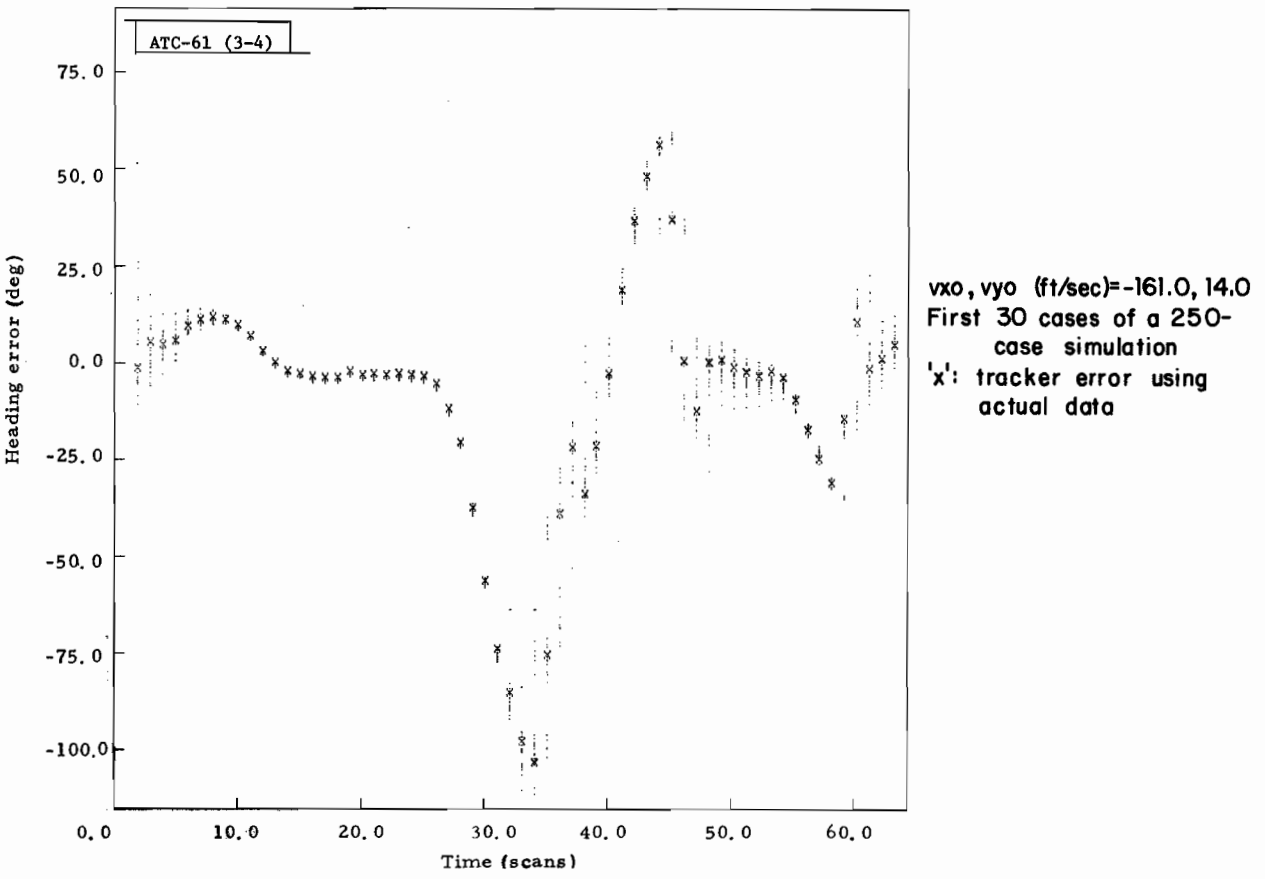

Fig. 3-4. Heading error vs scan for s-maneuver as illustrated in Fig. A-5.

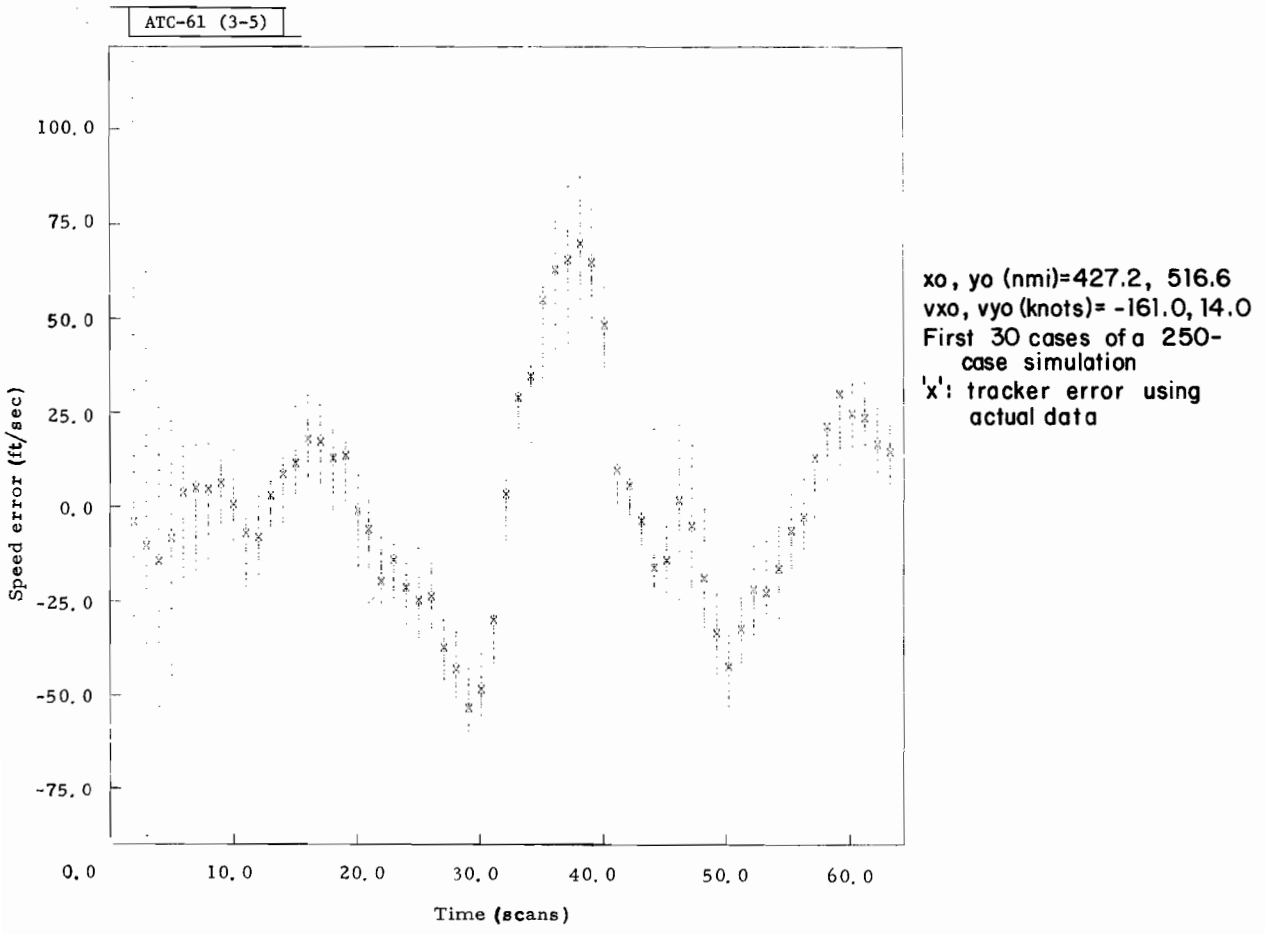

Fig. 3-5. Speed error vs scan for s-maneuver as illustrated in Fig. A-5.

In following the speed error profile, the speed estimate indicates a significant lead as the aircraft decelerates while going into the 7^{o}/sec turn. The subsequent acceleration while coming out of the turn, compounded by the delay in turn detection, causes the estimated speed to lag excessively. Near scan 35, the aircraft speed is approximately 100 ft/sec (Fig. A-6). In view of the fact that a lag in estimated speed of 75 ft/sec is indicated in the speed error profile (Fig. 3-5), the speed estimate during scan 35 is almost zero.

When the aircraft makes the final change in direction, the tracker has had enough time to recover from the last turn, and the turn detection process is not impeded. The turn detection delay is a normal 5 scans for the final 2.5^{o}/sec turn. The rapid turn with the associated speed changes, followed by a directional change, demonstrates a capability for testing the limits of the tracker. Although the maneuver is not typical, the excessive heading lag and speed errors that are developed indicate an area of tracker weakness.

3.2 Straight Line Tracker Performance

For a large portion of their flight time, aircraft follow paths that can be referred to as 'straight line.' The ability of an aircraft to follow an ideal straight line depends on wind condition, visibility, type of navigation equipment, and the size and type of aircraft. In this section 'straight line' flights are arbitrarily defined as flights that include all paths that 'wander' about a straight line with a turn rate less than 0.4/deg sec. This is realistic and permits a continuum in tracker performance evaluation between the turn rates considered in Section 2.0 and the ideal straight line cases.

As a result of the fact that speed estimates are of second order for low turn rates (refer to Section 2.4.2), heading performance will be used as a measure of tracker quality for 'straight line' trajectories. Figures 3-6(a) and 3-6(b) illustrate the rms heading error at ranges of 20 nmi and 40 nmi, respectively. The standard trajectory is used in a 250-case simulation. The rms value of the heading error is determined from 250 cases for the duration of the time that it takes the heading error to reach a steady state. Because only the linear portion of the tracker is utilized for low turn rate operation, the settling time (10 scans from start of turn) depends on only the filter time constant. Figure 2-5(d) provides an example of dynamic operation in the linear region.

Data uncertainties and the heading lag produced by the turn contribute to the error in estimated heading. It was pointed out in Section 2.4.2 that, for ideal data conditions, heading errors are independent of speed in the linear region. This is evident in Figs. 3-6(a) and 3-6(b) where, at the higher turn rates, the heading lags dominate which causes the performance curves at various speeds to converge. The heading lag developed in a turn is independent of both the orientation and range of the trajectory for operation in the linear region; this is not true for the heading caused by data uncertainty. Because the cross-track data uncertainty varies with both range and orientation,

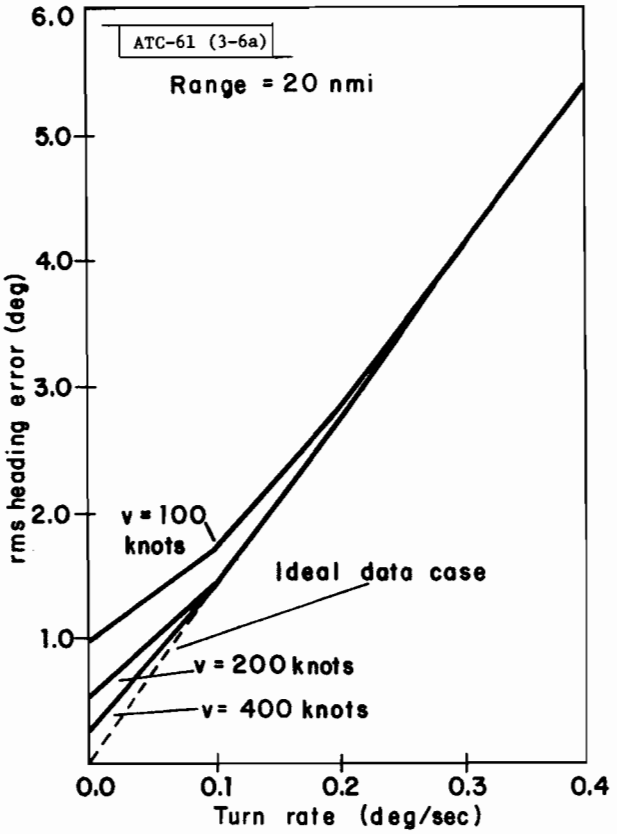

Fig. 3-6(a). Heading error vs turn rate for "straight line turn" (20 nmi).

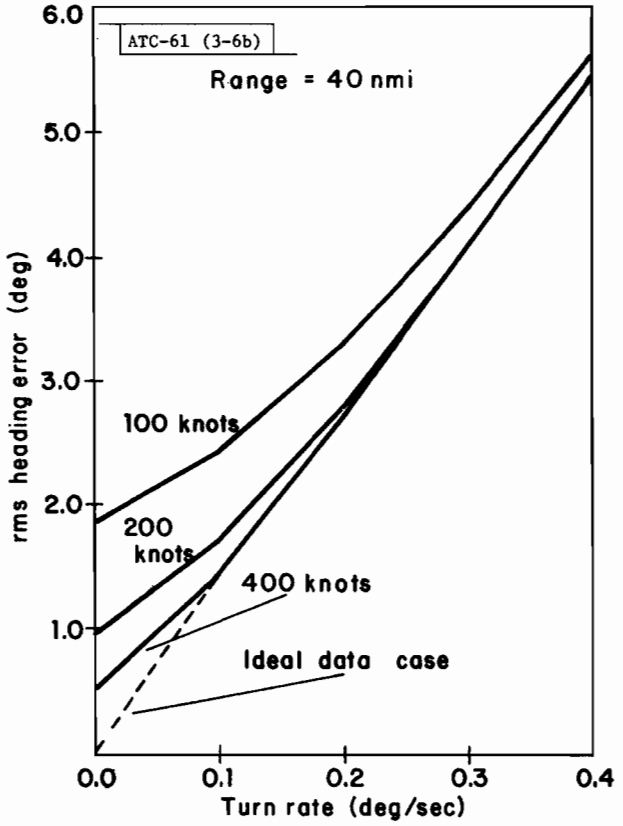

Fig. 3-6(b). Heading error vs turn rate for "straight line turn" (40 nmi).

(Tables B-1 and B-2), the heading uncertainty is a function of those factors. It can be demonstrated that the one standard deviation heading uncertainty, σ_h, can be defined by the equation:

$$\sigma_h = \sin^{-1} \frac{\sigma_c \beta}{vT} \sqrt{\frac{2}{\alpha(4-2\alpha-\beta)}}$$

where

σ_c = cross-track data uncertainty

T = scan time

v = speed of aircraft

α, β = gains of linear filter

The zero-turn rate errors indicated in Figs. 3-6(a) and 3-6(b) can be verified using this equation, e.g., consider a 100-knot turn at 20 nmi:

$$\sigma_c = .04^\circ \times \left(\frac{\pi}{180}\right) \times (20 \text{ nmi}) \times \left(6076 \frac{\text{ft}}{\text{nmi}}\right) \approx 85 \text{ ft}$$

v = 100 knots $\approx$170 ft/sec

α = 0.4

β = 0.1

$\sigma_h \approx 0.9$

The result of this calculation closely approximates the value indicated in Fig. 3-6(a). Using the preceding equation and the ideal data curve plotted in Fig. 3-6(a), the heading error for an arbitrary orientation and range can be constructed.

An example of controlled straight line flight was performed as part of the station keeping experiments at DABSEF. For part of the experiment a pilot flew a Cherokee-6 aircraft along a radial path in relation to the sensor using RNAV equipment. To evaluate the tracker under these conditions, a standard third-order polynomial curvefit, with a window size of 9 scans, was applied to the data. Figures 3-7(a) and 3-7(b) illustrate the probability

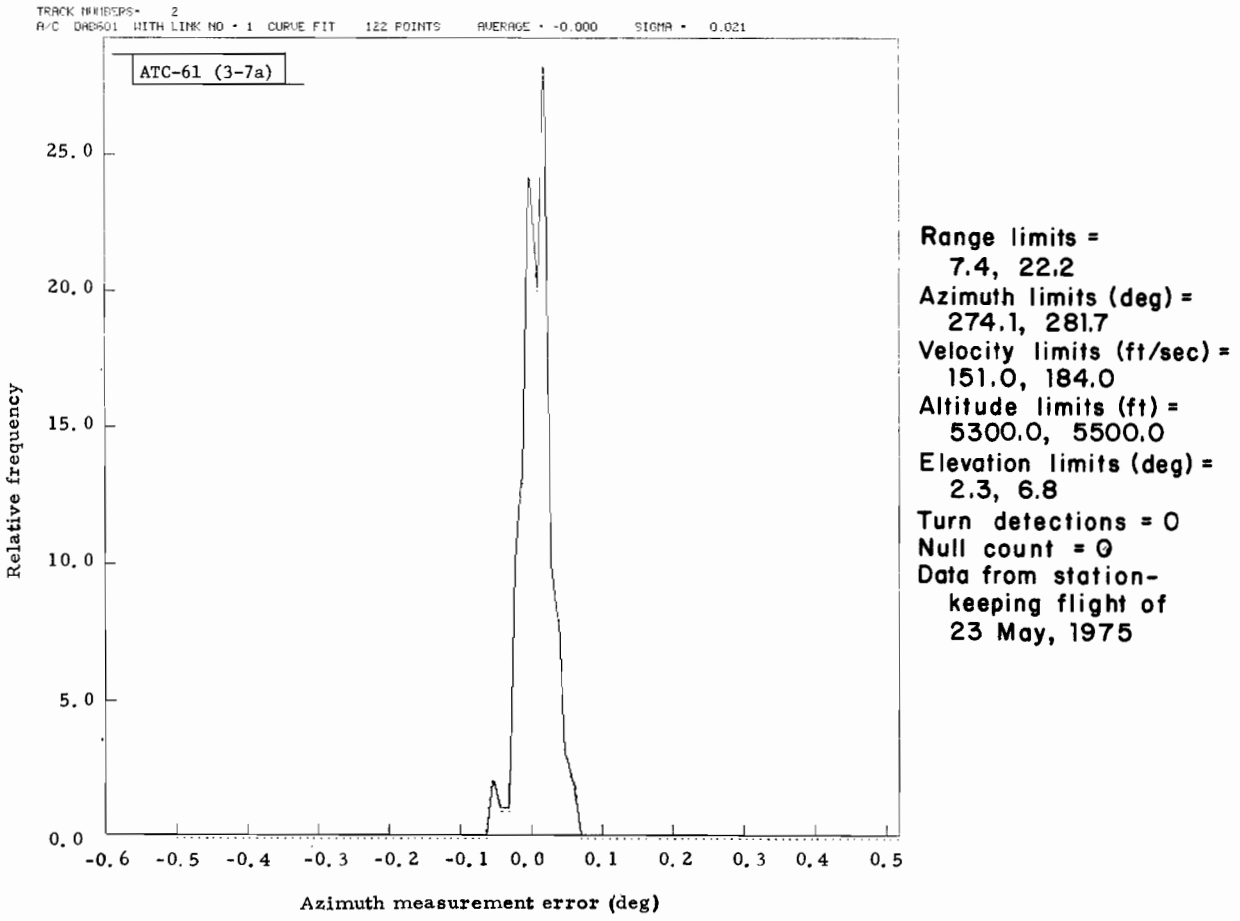

Fig. 3-7(a). PDF of azimuth data for straight line flight of 23 May 1975.

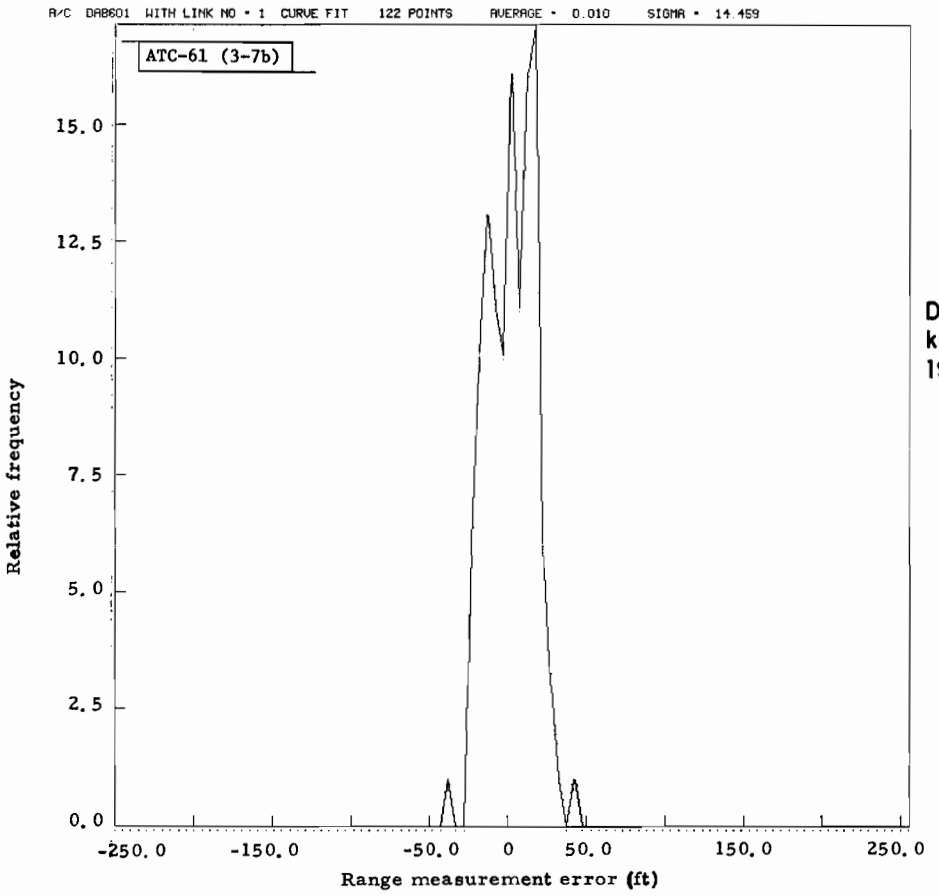

Data from station-keeping flight of 23 May 1975

Fig. 3-7(b). PDF of range data for straight line flight of 23 May 1975.

density distributions (PDFs) for the range and azimuth data obtained from the curve fitting. Note that, for this case, the quality of the data is better than the 0.04-degree and 30-ft uncertainties of the azimuth and range, respectively, assumed for the simulations. Figure 3-7(c) is a plot of the PDF for the heading error, which was obtained by comparing the heading derived from the curvefit coefficients and the heading derived from the tracker estimates.

The number to the right of Fig. 3-7(a) indicate the radial trajectory of the 23 May 1975 flight. Speed limits during the flight are based on speed estimates; the other limits referenced on Fig. 3-7(a) are derived from the sensor measurements. For an ideal radial flight, the azimuth and heading variations would be zero. For this actual case, the azimuth limits have a spread of 7.6 degrees. The significant heading error variance of approximately 3 degrees illustrated in Fig. 3-5 indicates a 'wandering' of the aircraft from a straight line path. The bimodality of the heading error distribution is caused by the change in polarity of the estimated heading lag as the aircraft changes direction. The results of ideal trajectories indicate that heading effects are related to the turn rate of the aircraft. It is arbitrarily assumed that the aircraft 'wandering' for this case is sinusoidal with a low frequency, and that the cumulative rms heading error to the peak heading deviation is 2 degrees. Referring to Fig. 3-6(a), a turn rate of 0.15^{o}/sec is indicated in correspondence to the cumulative rms error of 2^{o}. This controlled radial flight example is a case of tracker performance for a 'straight line' trajectory. It indicates that the performance is appreciably less satisfactory than for an ideal straight line flight.

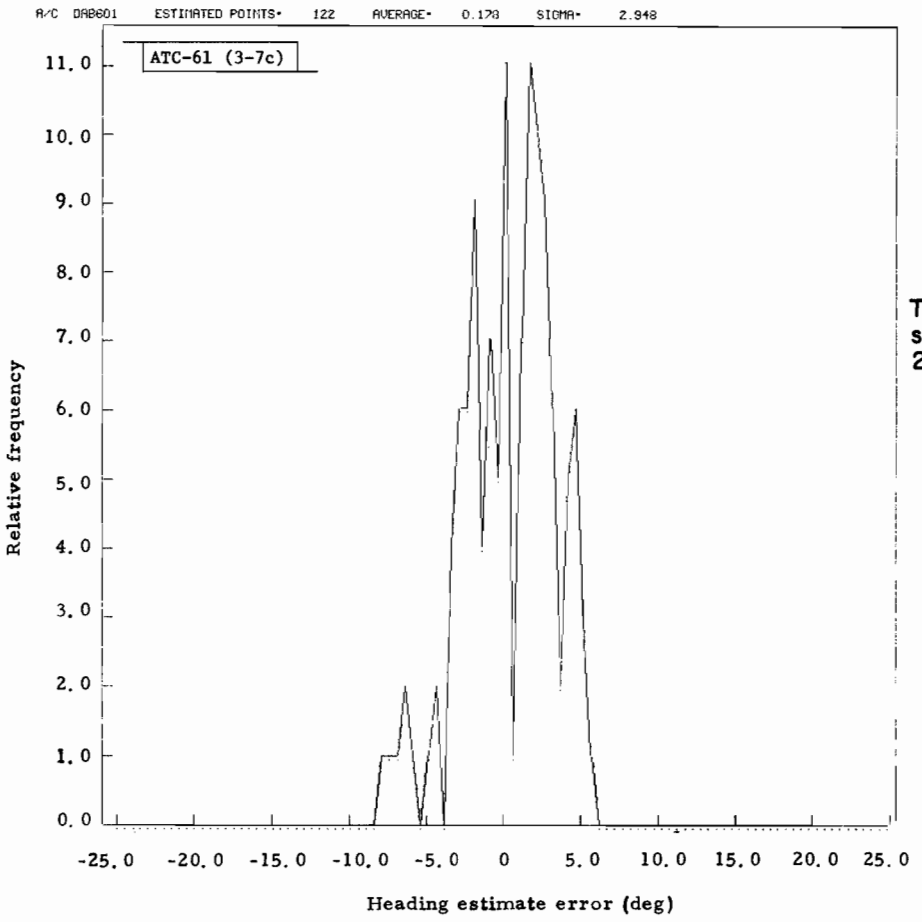

Tracker estimates from station-keeping flight of 23 May 1975

Fig. 3-7(c). PDF of heading estimate for straight line flight of 23 May 1975.

4.0 CONCLUSIONS AND POTENTIAL TRACKER IMPROVEMENTS

4.1 Conclusions

The IPC tracker simulations that were performed during this study, using both ideal and reconstructed real turn trajectories, support the following conclusions for the specified tracker:

(a) Heading Error
1. Heading errors during a turn are strongly dependent upon early and consistent turn declaration.

2. Heading error profiles are highly nonlinear with speed and tend to become constant during high-speed turns.

(b) Speed Error
1. Speed error profiles (for a given constant speed) tend to increase linearly with turn rate.

2. Normalized speed errors are approximately independent of speed.

3. Speed errors become more significant for aircraft exhibiting linear acceleration.

(c) Combined Effect of Turn Rate and Speed
1. Rapid turn rates and large speed change during a turn may cause unacceptable heading and speed errors.

2. Low turn rates, combined with low speeds, produce particularly large error fluctuations as a result of the data noise sequences introduced.

(d) Position Error
1. A projected rms position error of less than 3500 ft at a range of 20 nmi may be expected for the tracker studied if a 30-sec projection time is used. This error increases at greater ranges as a result of accumulated lag in the heading estimate prior to turn detection.

(e) Tracker Tuning
1. The present tracker is tuned to approximately 4.5^{o}/sec turn rate, which is somewhat higher than rates expected for most aircraft.

2. If turn declaration is maintained during a turn, tuning is independent of aircraft speed and range or threshold magnitude.

4.2 Potential Tracker Improvements

(a) Reducing the "heading error tuning point" to a lower value*, which would more nearly match turning rates expected for most aircraft, would decrease heading error.

(b) Use of the wind vector to adjust estimated velocity would improve speed performance. This would become a significant improvement if acceleration becomes a dominant factor after introduction of decreased threshold parameters.

(c) Decreased threshold parameters, permissible with improved surveillance accuracy (as has been demonstrated at DABSEF), would allow the tracker to utilize more fully the mechanisms of heading correction (especially tuning). With smaller thresholds, delays in turn detection and, therefore, heading lag would decrease and projected position accuracy would improve.

*Lower turning rate (less than the present value of 4.5^{o}/sec).

APPENDIX A

SIMULATION TRAJECTORIES

Four turn trajectories were utilized during the tracker performance simulation runs: (1) a simple 15-scan turn in a zero-wind field at constant altitude and speed, (2) a simple 180-degree turn from a downwind leg to an upwind parallel leg, (3) an s-shaped turn, and (4) an ampersand (&)-shaped turn.

A.1. Ideal Reference Turn

The first turn, referred to as the "ideal turn," is illustrated in Fig. A-1. This trajectory is constructed from segments of straight lines and perfect circles. Assumptions permitting this construction were:

(a) The aircraft flies at constant speed and altitude.

(b) Upper air winds do not exist.

(c) Linear accelerations do not occur.

(d) The aircraft turn rate is constant.

(e) The surveillance sensor scans at a constant 4-second/scan rate.

A.2. 180° Turn in a Wind Field

The 180° turn and the s-and ampersand-shaped turns are non-ideal trajectories based upon smoothing surveillance data obtained during actual IPC encounter flights. The trajectories are reconstructed by using a standard third-order polynomial curvefitting technique. A window size of five scans is used in the curvefitting if, during any scan in the window, the real time IPC tracker has declared a turn; otherwise a window size of seven scans is assumed. The curvefit trajectory is used to construct noisy tracks for the simulation.

The 180° turn trajectory represents the case of an aircraft turning in the wind. Figure A-2 illustrates such a curvefit trajectory that starts with a 180-degree turn at a rate of 6°/sec flying downwind. At the end of the turn, the aircraft is flying against the wind. The wind has distorted the turn and also caused the aircraft to lose ground speed. Figure A-3 is a plot of a speed profile (obtained from the curvefit)* for the aircraft and indicates a change in speed of approximately 70 knots.

*The error associated with the speed curvefit is of the order of 10 ft/sec.

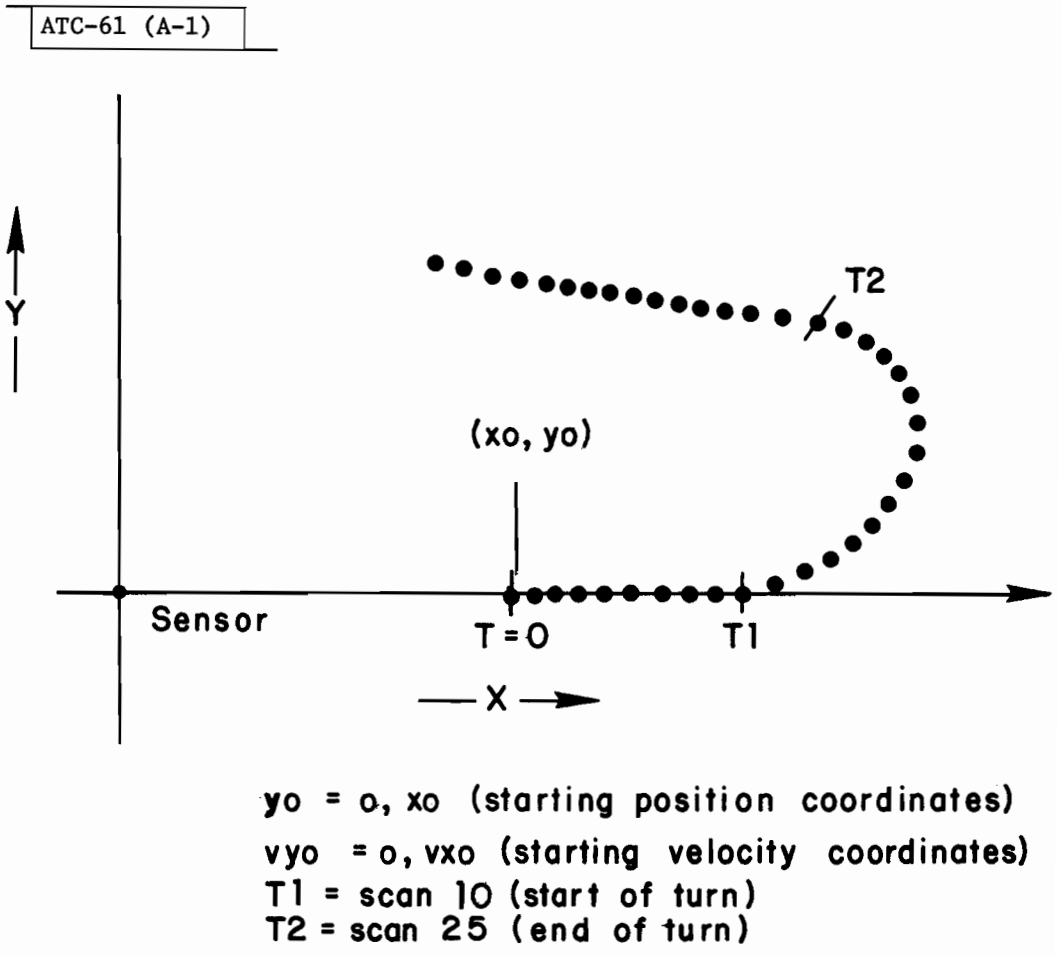

Fig. A-1. Reference turn used during tracker simulations.

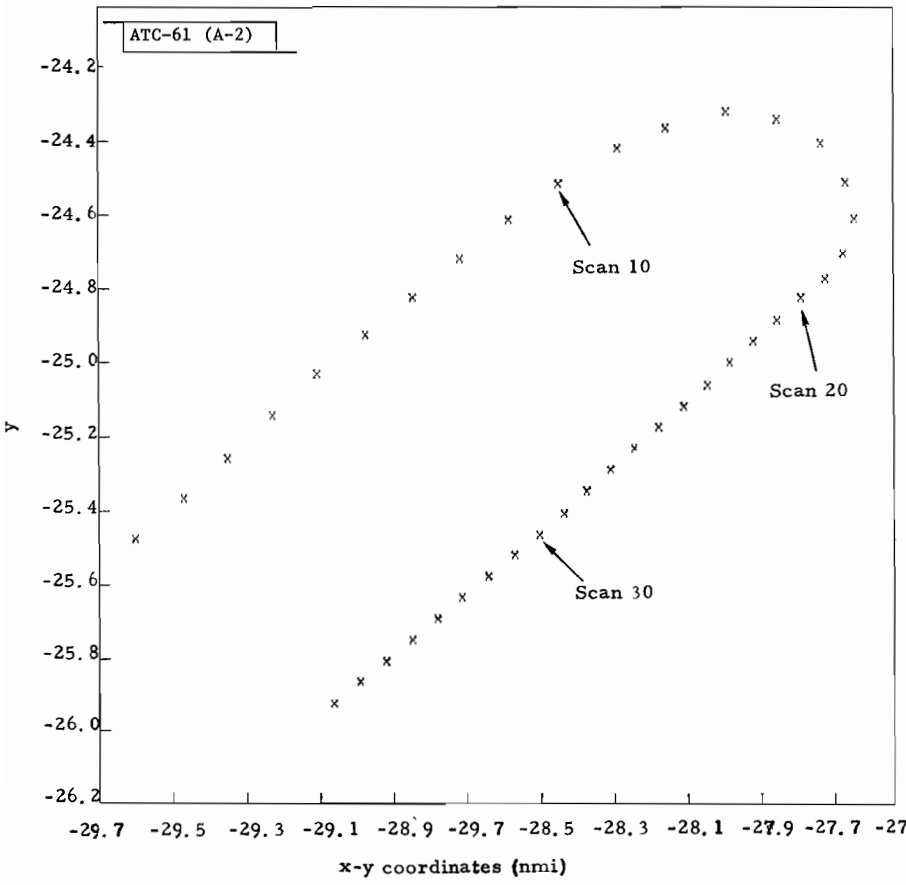

Curvefit trajectory from data obtained during a station-keeping flight of 23 May 1975;
A/C DABS equipped with ID = DAB601

Fig. A-2. Reconstructed actual turn (Cherokee turning in wind).

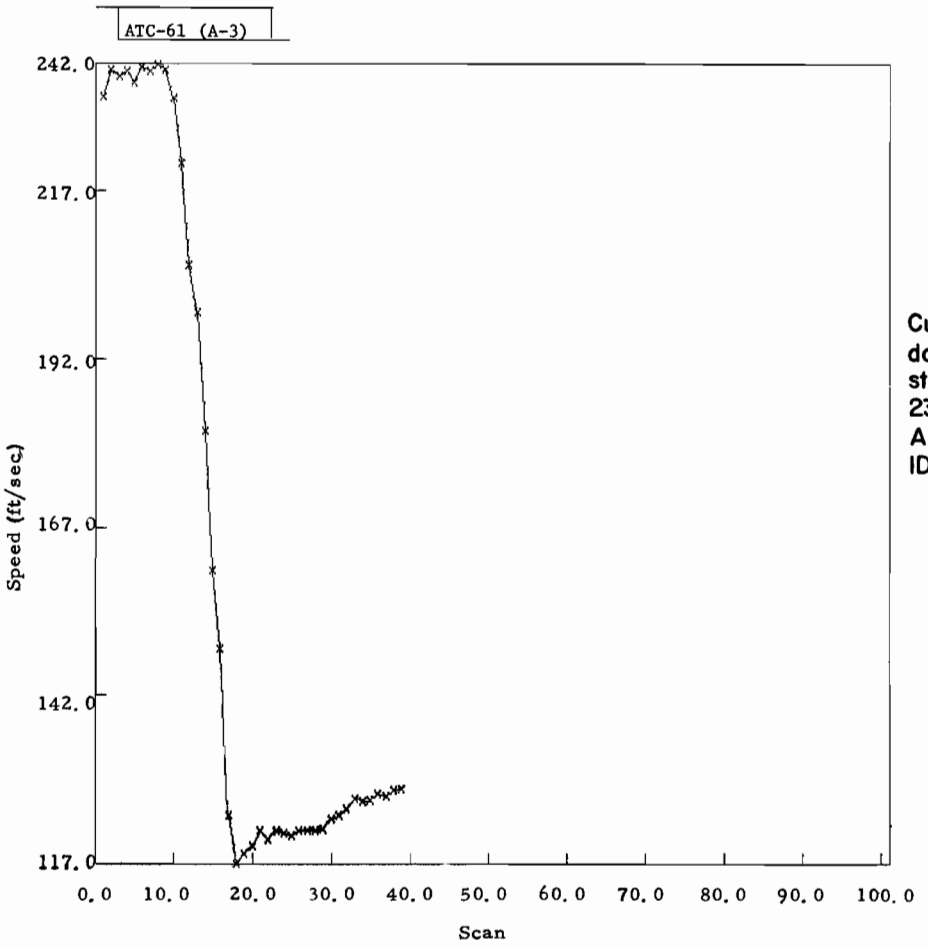

Curvefit speed profile from data obtained during a station-keeping flight of 23 May 1975;
A/C DABS equipped with ID = DAB601

Fig. A-3. Speed vs scan for turn illustrated in Fig. A-2.

A.3. S-and Ampersand-Shaped Turns

The s-and ampersand-shaped turns are also non-ideal reconstructed actual turns. Each of these turns is illustrated in Figs. A-4 and A-5, respectively. Speed and heading vs scan number for the ampersand turn are indicated in Figs. A-6 and A-7.

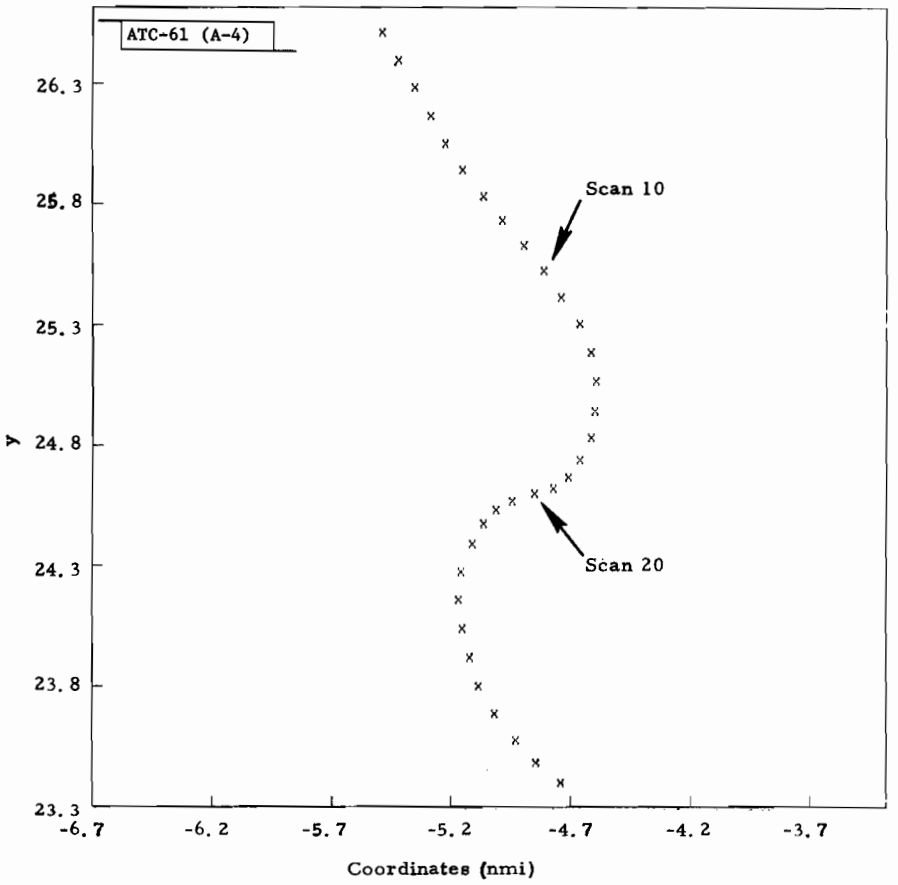

Curvefit trajectory from data obtained during IPC flight IPC 172;
A/C DABS equipped
ID = DAB101
Scans 97 to 129

Fig. A-4. Reconstructed s-maneuver flown during an IPC test flight.

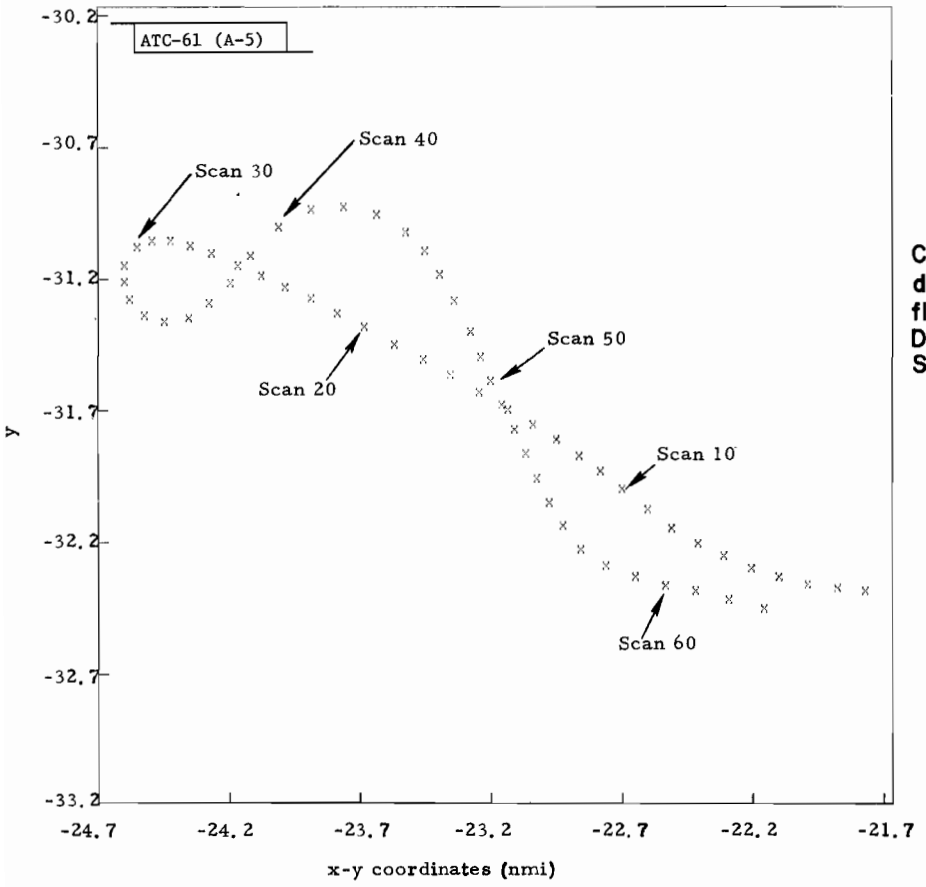

Curvefit trajectory from data obtained during IPC flight IPC 156;
DABS ID = DAB101
Scans 17 to 79

Fig. A-5. Ampersand maneuver of IPC flight 156

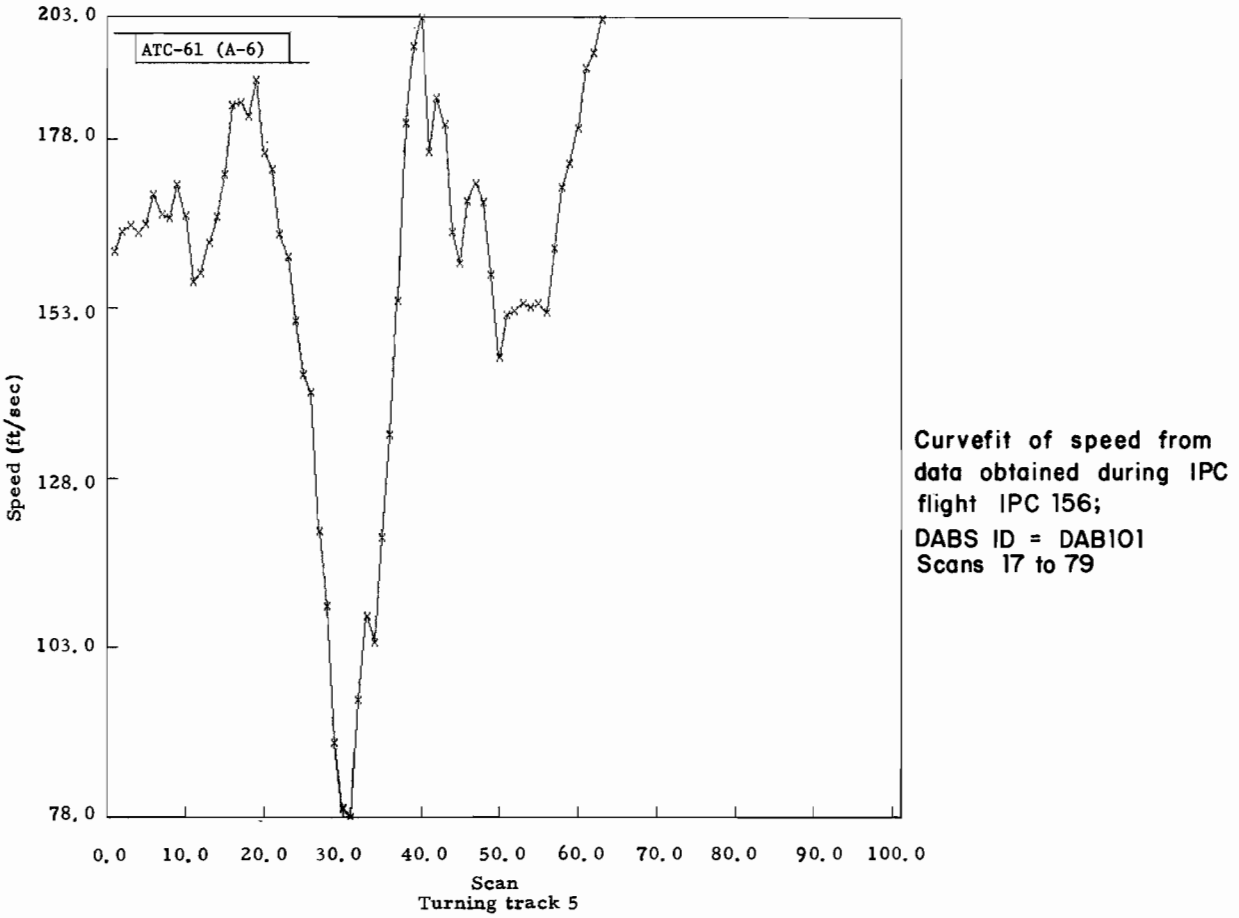

Fig. A-6. Heading vs scan for ampersand maneuver as illustrated in Fig. A-5.

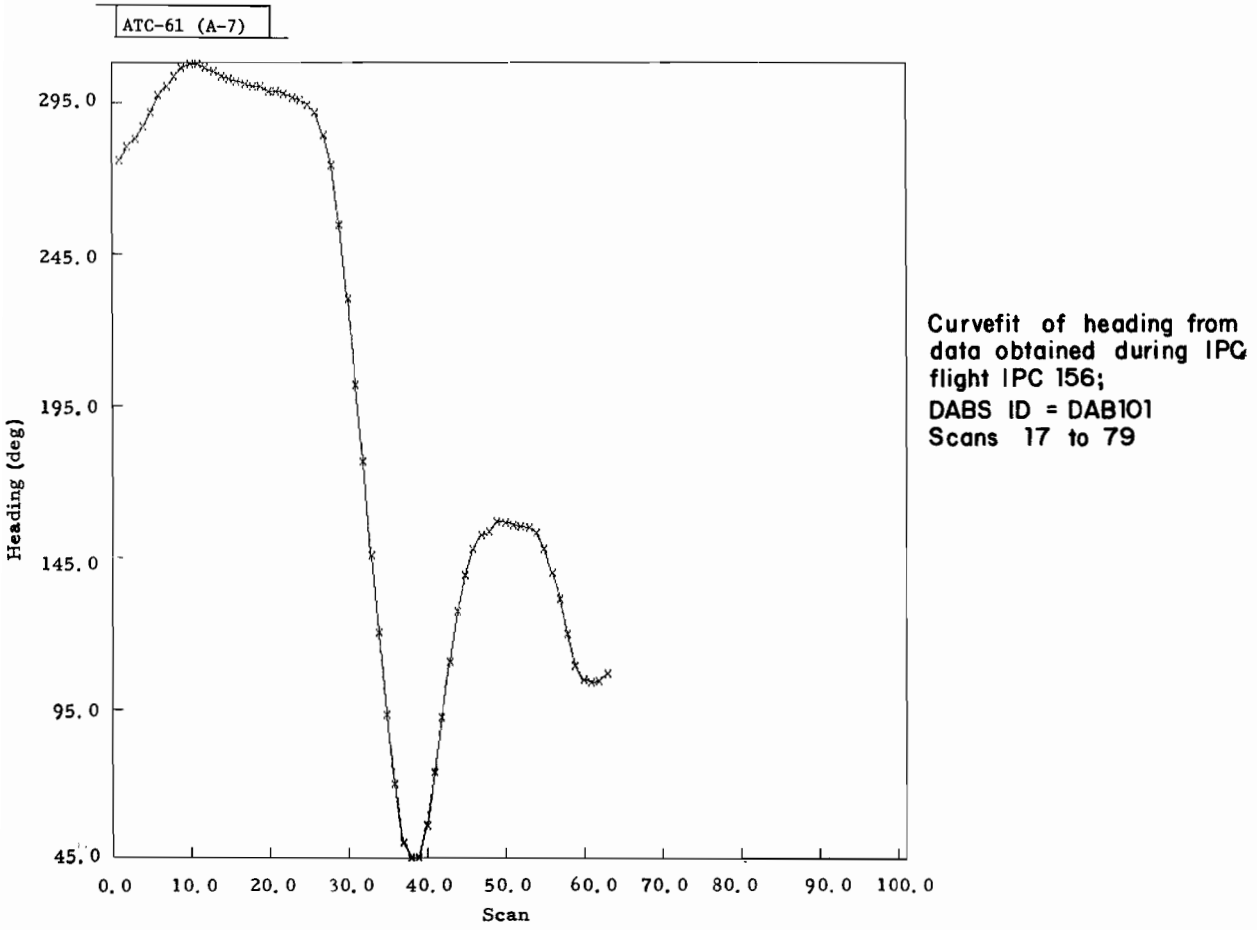

Fig. A-7. Heading vs scan for ampersand maneuver as illustrated in Fig. A-5.

APPENDIX B

TURN DETECTION MECHANISM

This Appendix explains turn detection in order to aid the reader in understanding tracker behavior. If no turn detection mechanism existed, the tracker would of course be an ordinary α-β tracker, and its characterization would be more simple. The nonlinear nature of the tracker is caused by the threshold mechanism used for detecting turns. If the threshold mechanism declares a turn, a correction is made to the tracker heading. The angle, γ, which is between the tracker heading and the heading obtained by using the last estimated internal position* and the new measurement, is calculated. For the initial turn declaration, a correction equal to $\gamma/2$ or 20° (whichever is smaller) is utilized. For the subsequent turn detection, a correction of $\gamma/2$ (20° max) + 15° is applied. The threshold used to declare the turn is a function of measurement uncertainties, heading, speed, and firmness and is calculated by

$$\text{threshold} = \text{THK}(I_f) \times (3.1\sigma_{CR} + 0.8v)$$

where

v = speed estimate (ft/sec)

σ_{CR} = amount of data uncertainty† along a direction perpendicular to the estimated velocity vector

$\text{THK}(I_f)$ = a scaling factor that is a function of firmness level (THK = 100 at startup; THK = 1 in steady state)

I_f = firmness level; this quantity represents the confidence level of the tracker estimates (I_f = 1.0 for steady state)

---

*Refer to Appendix C

†The performance of the x-y tracker has been simulated, and the tracker takes into account the specified DABS range and azimuth uncertainties of:

$$\sigma_R = 150 \text{ ft}$$
$$\sigma_{az} = 0.1 \text{ deg}$$

Actually, it has been determined that the measurement uncertainties at DABSEF are considerably smaller than the specified DABS values. In order to compare simulated and actual cases, the range and azimuth uncertainties determined during IPC flight tests at DABSEF have been used, i.e.:

$$\sigma_R = 30 \text{ ft}$$
$$\sigma_{az} = 0.04 \text{ deg}$$

Figure B-1 illustrates the parameters involved in deriving σ_{CR}. If the cross-track residue is greater than the threshold, a turn declaration is generated.

Using the parameters in Fig. B-1, the cross-track uncertainty, σ_{CR}, can be expressed by the equation

$$\sigma^2_{CR} = (R^2 \sigma^2_{az}) \cos^2\theta + (\sigma^2_R) \sin^2\theta$$

When interpreting results, it is useful to express the threshold as a function of heading and range for some specific cases. Table B-1 presents the threshold as a function of heading for an aircraft at 40 nmi, (with firmness = 1). Table B-2 presents the threshold as a function of range (with firmness = 1, $\theta_h = 90^o$ and 0^o).

Maximum cross-track uncertainty (σ_{CR}) occurs at either $\theta_h = 0^o$ or $\theta_h = 90^o$, depending upon whether or not the range uncertainity or cross-range uncertainty is dominant. For a range

$$R = \frac{\sigma_R}{\sigma_{az}}$$

the cross-track uncertainty becomes independent of heading. For tracker uncertainties of $\sigma_R = 150$ and $\sigma_{az} = 0.1^o$, this occurs at 14 nmi. For aircraft at greater range, $R\sigma_{az}$ becomes dominant, and the maximum threshold occurs when the aircraft heading is oriented along the sensor radial vector ($\theta_h = 0$). The dependence of the threshold to track orientation and range is indicated by the data in Tables B-1 and B-2. Note that in Table B-2, with $\theta_h = 0$, the cross-track error is independent of range. For this case, the aircraft heading is along a direction normally radial; as a result, the cross-track direction is along the radial. Because it is assumed that the range uncertainty (σ_R) is independent of range, the cross-track uncertainty for this case also becomes independent of range.

The orientation of the basic simulation turn illustrated in Fig. A-1 is designed to maximize the turn detection threshold for the slated initial conditions. For the majority of the summary graphs presented, the initial range is greater than 14 nmi.

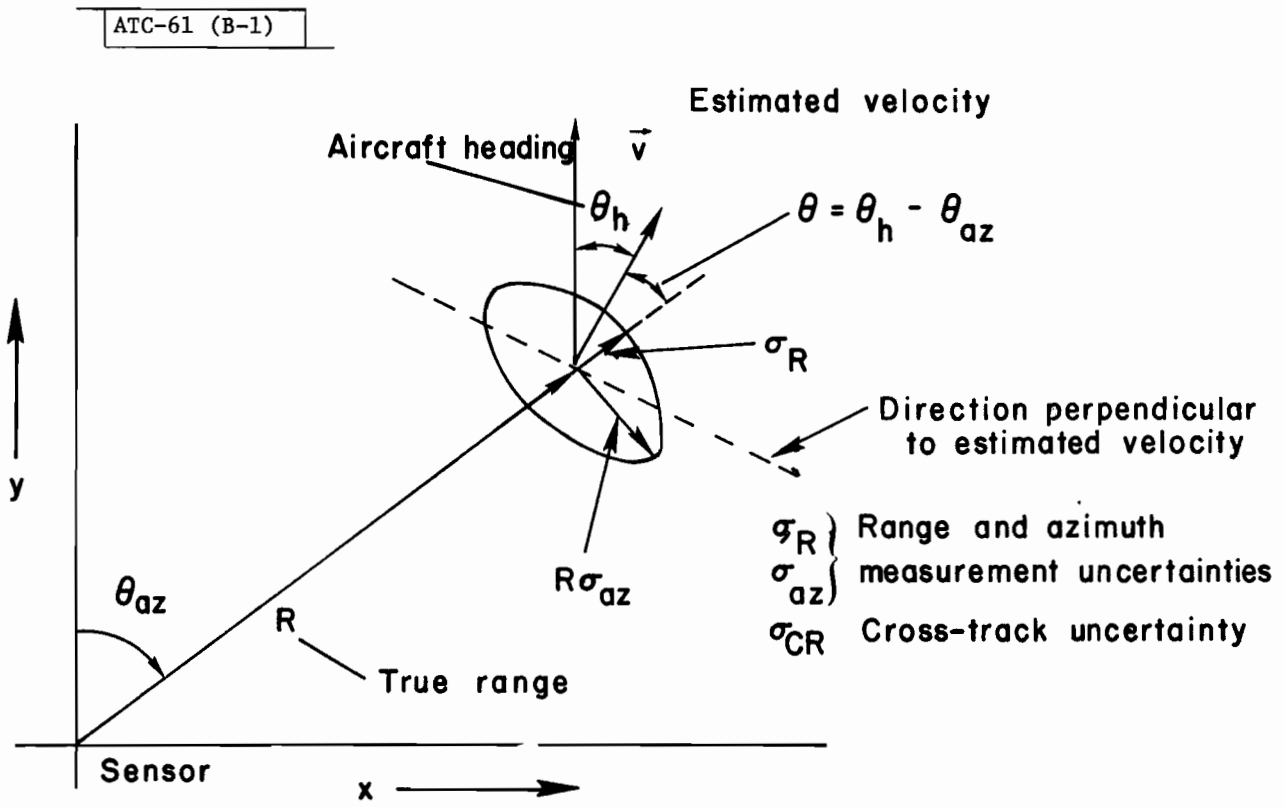

Fig. B-1. Cross-track uncertainty.

TABLE B-1. THRESHOLD AS A FUNCTION OF HEADING

Heading (deg)	σ_{CR} (ft)	Threshold (ft)
0	150	735
30	249	1042
60	375	1433
90	425	1588

X0 = 40 nmi

Y0 = 0

Speed = 200 knots

$\theta_{az} = 90^{o}$

TABLE B-2. THRESHOLD AS A FUNCTION OF RANGE

Range (nmi)	$\theta_h = 90^{o}$		$\theta_h = 0^{o}$	
	σ_{CR} (ft)	Threshold (ft)	σ_{CR} (ft)	Threshold (ft)
10	106	464	150	600
20	213	795	150	600
30	319	1124	150	600
40	425	1453	150	600
50	532	1784	150	600
60	638	2113	150	600

Firmness = 1.0

Speed = 100 knots

$\theta_{az} = 90^{o}$

APPENDIX C

x-y TRACKER EQUATIONS

The x-y tracker is described in detail in Ref. 1. The tracker equations are presented here in a summarized form. It is assumed that target-to-track correlation has been completed and that the tracking begins with the process of prediction.

Prediction:

$$XPI = XSI + DT * XDI$$
$$YPI = YSI + DT * YDI$$

$$XP = XS + DT * XDI$$
$$YP = YS + DT * YDI$$
$$ZP = ZS + DT * ZD$$

where:

XPI, YPI = internal predicted positions

XSI, YSI = internal smooth positions from the last scan

XDI, YDI = internal smooth velocities from the last scan

ZD = smooth z-velocity from last scan

DT = time that has elapsed since the last scan

XP, YP = external predicted positions

XS, YS = external smooth positions from the last scan

ZS, ZP = for z-axis the smooth position from last scan, and predicted position for this scan, respectively

Computation of residues:

$$DIX = XM - XPI$$
$$DIY = YM - YPI$$

$$DEX = XM - XP$$
$$DEY = YM - YP$$
$$DEZ = H - ZP$$

where:

DIX, DIY = internal filter residues

XM, YM = cartesian ground components of the range and azimuth data

DEZ = z-residue

DEX, DEY = external filter residues

H = altitude measurement

$$DRX = XM - XSI$$

$$DRY = YM - YSI$$

where:

DRX, DRY = components of a vector that is parallel to a velocity derived from the last internal smooth position and the current measurement

Cross-track position deviation:

$$B = XDI * XDI + YDI * YDI$$

$$A = DX * YDI - DY * XDI$$

$$S = A / ABS(A)$$

$$D2 = A*A / B$$

where:

B = the square of internal speed estimate

D2 = the square of the cross-track positional deviation

S = sine of A

Internal smoothing:

$$XSI = XPI + ALXY\ (FRMI) * DIX$$

$$YSI = YPI + ALXY\ (FRMI) * DIY$$

$$XDI = XDI + BEXY\ (FRMI) * (DIX/DT)$$

$$YDI = YDI + BEXY\ (FRMI) * (DIY/DT)$$

where:

XSI, YSI = current smooth internal positions

XDI, YDI = current smooth internal velocities

ALXY, BEXY* = linear filter gains, which are a function of firmness

FRMI = internal firmness (varies from 1 to 9)

External smoothing:

$$XS = XP + ALXY\,(FRME) * DEX$$
$$YS = YP + ALXY\,(FRME) * DEY$$

where:

XS, YS = current smooth external positions

FRME = external firmness (varies from 1 to 4)

z-smoothing:

$$ZS = ZP + ALXY\,(FRMZ) * DZ$$
$$ZD = ZD + BEXY\,(FRMZ) * (DZ/DT)$$

where:

ZS, ZD = current smooth values of z-position and z-velocity, respectively

FRMZ = z-firmness (varies from 1 to 7)

Threshold computation*:

$$D2Th = THK(FRMI) * \left(DTHA + DTHB * \frac{(XSI * XDI + YSI * YDI)^2}{V2I * R2I}\right)$$

where:

R2I = XSI * XSI + YSI * YSI

V2I = XDI * XDI + YDI * YDI

and:

$$DTHA = (3.1 * STDA + 1.35 * \sqrt{V2I})^2$$
$$DTHB = (3.1 * STDC + 1.35 * \sqrt{V2I})^2 - DTHA$$

---

*For values of gains as a function of firmness, see Ref. 1.

where:

STDA, STDB are the positional along-range and cross-range data uncertainties

V2I is the smooth value of current speed estimate (knots)

At this point, a trial is made to determine whether or not the square of the cross-track deviation, D2, exceeds the threshold D2TH. If a turn is sensed, a correction in the direction of the sensed turn is made.

Calculate the angular offset corresponding to the vectors (DRX, DRY) and (XDI, YDI):

$$C = DRX * XDI + DRY * YDI$$

$$P = \text{Sign } (C)$$

$$CP2 = C*C/(V2I*(DRX*DRX + DRY*DRY)$$

where:

CP2 is the square of the cosine of the angular offset.

$$CP = \sqrt{CP2}$$

$$CDT = \sqrt{((1+CP)/2)}$$

$$SDT = \sqrt{((1-CP)/2)}$$

where:

CDT, SDT = cosine and sine of half the angular offset.

A correction, based on the angular offset, is made to the current internal smooth velocity vector. If the angular offset exceeds 40 degrees, a correction of 20 degrees is applied; otherwise, the smooth velocity is corrected by half the angular offset.

Angular correction to smooth internal velocity:

$$XDI = XDI*CDT + S*YDI*SDT$$

$$YDI = YDI*CDT - S*CDI*SDT$$

$$YDI = XDI$$

where:

CDT and SDT are the cosine and sine of the half-angle offset or 20 degrees, whichever is smaller.

An external velocity vector is generated for IPC use only; it does not in any way affect the threshold mechanism or the internal filter. In cases where the current and last turn detection are of the same polarity, the external velocity vector is generated by rotating the internal velocity an additional 15 degrees:

$$XDE = XDI*CDEL + S*YDI*SDEL$$

$$YDE = YDI*CDEL - S*XDI*SDEL$$

where:

CDEL, SDEL are cosine and sine of 15 degrees, respectively

In cases where a turn has not been detected during this scan, or the polarity S of the current turn detection does not concur with that of the last scan:

$$XDE = XDI$$

$$YDE = YDI$$

Firmness values are not affected by turn detection in any way. For more information pertaining to how firmness levels are affected by data, including the absence of data, refer to the IPC Tracker section in Ref. 1.

REFERENCES

[1] "A Description of the Intermittent Positive Control Concept," FAA-EM-74-1, Rev. 1 dated July 1975.

[2] A. L. MacFarland, "Multi-site, IPC Algorithms for the Discrete Address Beacon System," MITRE Corp., Report CMTR-6742, FAA EM-74-4 (September 1974).